Macromolecules

Rheology and Pinching Dynamics of Associative Polysaccharide Solutions

Carina D. V. Martínez Narváez, Jelena Dinic, Xinyu Lu, Chao Wang, Reza Rock, Hao Sun, and Vivek Sharma*

Cite This: *Macromolecules* 2021, 54, 6372−6388

Read Online

ACCESS | Metrics & More | Article Recommendations

ABSTRACT: Associative polysaccharides, decorated by multiple but short, side-chain hydrophobic stickers (typically 6−20 carbon long) that associate in solution, are used as thickeners for an extensive range of aqueous-based formulations. Characterizing and elucidating the influence of stickers on the response to extensional flows that spontaneously arise in pinching necks formed during spraying, jetting, or coating fluids have remained longstanding experimental and analytical challenges due to relatively low viscosity and elasticity of industrially relevant systems. In this contribution, we contrast the shear rheology as well as extensional rheology and pinching dynamics of hydrophobically modified hydroxyethyl cellulose (hmHEC, M_w = 300 kg/mol) as a sticky polymer with the bare chain of a higher molecular weight (hydroxyethyl cellulose (HEC), M_w = 720 kg/mol) using the recently developed dripping-onto-substrate (DoS) rheometry protocols. We show that sticker associations enhance zero shear viscosity and relaxation time (elasticity), and both quantities display stronger concentration-dependent variation for sticky polymers. Striking differences are observed in neck shapes, radius evolution profiles, and extensional viscosity plotted as a function of strain as well as strain rate. We present a comprehensive analysis of changes in pinching dynamics, concentration-dependent variation in steady, terminal viscosity as well as filament lifespan as a function of the sticky polymer concentration and describe the influence of multiple stickers on the macromolecular strain, relaxation, and dynamics of associative polysaccharides.
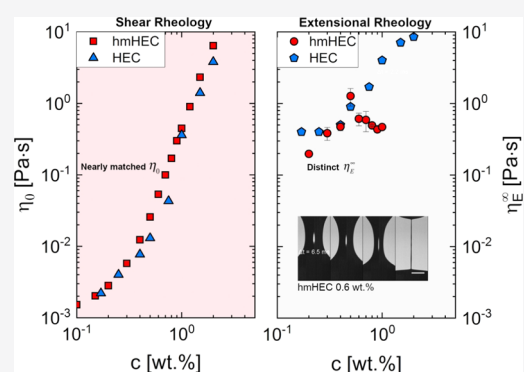

INTRODUCTION

Hydrophobically associative polymers are a commercially important subclass of water-soluble polymers,[1−5] with a relatively long hydrophilic backbone (macromolecules, with typical molecular weights >20 kg/mol), decorated with short, side-chain hydrophobic stickers (typically 6−20 carbon long). In aqueous dispersions, hydrophobic stickers located at chain ends (telechelic), or sparsely distributed along the chain (nontelechelic), self-assemble to minimize their exposure to water.[1−5] The association of stickers creates reversible intra- and inter-chain hydrophobic junctions that break and reform continuously due to thermal fluctuations and applied deformations.[1−7] Macromolecular dynamics, slowed down by association of stickers, manifest as an increase in shear viscosity, relaxation time, and elasticity, as well as change in rate-dependent shear viscosity (both shear thinning and thickening) and increase in frequency-dependent moduli for sticky polymers compared to the corresponding bare chains.[1−8] The hydrophobic associations drive the formation of clusters that grow with concentration, eventually forming transient networks.[6−11] Physically crosslinked hydrogels containing such hydrophobic or other forms of associations (hydrogen

bonding, ionic, van der Waals, metal co-ordination) have nonlinear rheological behavior and mechanical properties suitable for applications in drug delivery, tissue engineering, actuation, self-healing, food formulations, and stimuli-responsive materials.[11−22] Here, we restrict our attention to the dynamics and rheology of nontelechelic, multisticker, hydrophobically associative polysaccharides, used as rheology modifiers or thickeners for an extensive range of aqueous-based formulations including inks, paints, pharmaceuticals, cosmetics, drilling fluids, foods, and coating dispersions.[1−4,14] We address the longstanding challenges for characterizing the extensional rheology, pinching dynamics, and processability of hydrophobically modified or sticky polymers and corresponding bare chains. We utilize dripping-onto-substrate (DoS) rheometry protocols we developed[23−30] to characterize
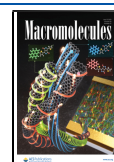
capillarity-driven pinching dynamics and extensional rheology of solutions of an associative polysaccharide, a hydrophobically modified hydroxyethyl cellulose (hmHEC), and its bare chain counterpart, hydroxyethyl cellulose (HEC).

The shear rheological response and the relaxation dynamics of hydrophobically modified analogues of carboxymethylcellulose (CMC),[31] hydroxyethyl cellulose (HEC),[32−40] ethylhydroxyethyl cellulose (EHEC),[5,41−43] polysaccharide intercellular adhesin (PIA),[44] carboxymethyl pullulan,[45] dextran,[46] chitosan,[47−50] cellulose octanoate sulfate,[51] and guar gum[52] have been investigated and reviewed before.[19,20] As rheology modifiers for commercial paints and coatings, associative polysaccharides are known to outperform unmodified counterparts in the qualitative comparisons of dispersion stability (thickening effect) due to a significant shear viscosity enhancement at low deformation rates. Likewise, stronger shear viscosity reduction for associative polysaccharides facilitates higher deformation rate processing and dispensing operations like roller coating, doctor blading, brush applications, and spraying. However, differences in sprayability, jettability, spinnability, ropiness, stringiness, and tackiness observed during processing and applications as well as in heuristic tests (like dripping from a spoon or stretching liquid bridge between a finger and thumb) cannot be typically inferred or explained using the knowledge of shear rheology response.[5,23−25,27−30,53−55] Multicomponent fluids that are sprayed, ink-jet printed, or roller coated all encounter strong extensional flows associated with streamwise velocity gradients that spontaneously arise within pinching liquid necks during drop formation or near curved interfaces in coating flows.[53−57]

An interplay of inertial, viscous, and capillary stresses determines the pinching dynamics for Newtonian fluids,[57−60] but additional viscoelastic stresses, contributed by the macromolecular response to extensional flows, influence pinching rate and time for necks of polymeric complex fluids.[23−30,53,57,61−64] It is well established that the knowledge of shear rheology response is not adequate to estimate or predict the strain and strain-rate-dependent extensional viscosity (also referred to as tensile stress growth coefficient), $\eta_E = \eta_E^+(t,\dot{\varepsilon})$ of solutions and melts of bare polymers, and shear-thinning systems can exhibit pronounced extensional hardening.[23−30,53−55,65] As the measurement of steady values, $\eta_E(\dot{\varepsilon}) = \eta_E^+(t,\dot{\varepsilon})$ $t \to \infty$ are relatively rare, often the plots show $\eta_E = \eta_E^+(t,\dot{\varepsilon})$ as a function of extensional strain, ε. High sensitivity to deformation history, flow instabilities, and limited range of accessible strain or strain rates pose practical challenges to extensional rheology characterization.[5,30,53,55,65−69] Therefore, only a few extensional rheology measurements exist for associative polymers, including for hydrophobically modified alkali-soluble emulsion (HASE) polymers[70] and measurements for associative polysaccharide solutions are even rarer (see Table 1).

In this contribution, we utilize hmHEC (M_w = 300 kg/mol) of lower molecular weight than bare chains (HEC, M_w = 720 kg/mol) such that the solutions of both have comparable shear viscosity at matched concentrations (discussed herein). We contrast the extensional rheology and pinching dynamics of hmHEC and HEC using dripping-onto-substrate (DoS) rheometry protocols[23−30] that rely on visualization and analysis of capillarity-driven pinching of liquid filaments (or necks) created by dripping a fixed volume of fluid onto a substrate. The Materials and Methods section summarizes specific challenges for characterizing pinching dynamics of poly-

saccharide solutions, recounts the success of DoS rheometry protocols in characterizing response from relatively low elasticity fluids, and tabulates the expressions used for analyzing pinching dynamics using radius evolution data to characterize material properties, including extensional viscosity and extensional relaxation time. In the Results and Discussion section, the steady shear rheology response of hmHEC solutions is described first, and concentration-dependent increase in zero shear viscosity and apparent shear relaxation time is contrasted against the corresponding values measured for HEC solutions. Thereafter, the contrast in pinching dynamics and extensional rheology response of HEC and hmHEC solutions is described using neck shapes and radius evolution data obtained using DoS rheometry. Striking differences observed in strain and strain-rate-dependent extensional viscosity are analyzed to elucidate the influence of multiple stickers on the macromolecular strain, relaxation, and dynamics. We anticipate that the comprehensive analysis of both shear and extensional rheology response of multisticker associative polymers presented here will inspire synthetic chemists to explore new chemical structures, industrial formulation scientists to use DoS rheometry for characterization and quality control, and polymer physicists and rheologists for developing deeper insights into dynamics of sticky chains and more robust constitutive models.

■ MATERIALS AND METHODS

Aqueous solutions of 2-hydroxyethyl cellulose (HEC) and a hydrophobically modified hydroxyethyl cellulose (hmHEC) commercially known as Natrosol Plus 330CS (Ashland) were prepared by slowly adding the polymer powder with no additional purification to deionized water. The solutions were then placed on a roller for more than 5 days to achieve homogeneous mixing and avoid high deformation rates that can lead to chain scission.[71−74] The average molecular weight for the bare polymer (HEC) is M_w = 720 kg/mol with molar substitution, M.S. = 2.5 (Sigma-Aldrich). The average molecular weight of the associative polymer (hmHEC) is M_w = 300 kg/mol, with M.S. = 2.5 of ethylene oxide groups per anhydroglucose unit (see Figure 1a). In contrast, hexadecyl or cetyl group (C-16) stickers (or hydrophobically associative groups) are included with a much lower M.S. = 0.01.[37,38,75] The association of stickers creates transient junctions shown schematically in Figure 1b.

The shear rheology response of polymer solutions was characterized using a concentric cylinder Couette cell for low-viscosity aqueous HEC and hmHEC solutions and cone-and-plate geometry (50 mm diameter, 1° cone angle) for higher viscosity aqueous solutions on an Anton Paar MCR 302 rheometer (torque range 10^{-5}−200 mN/m) at 25 °C. The steady shear viscosity, $\eta(\dot{\gamma}) \equiv \tau_{12}/\dot{\gamma}$, was calculated from the measured shear stress, τ_{12}, from imposed shear rates in the range of $\dot{\gamma}$ = 0.01−10^3 s^{-1}. The extensional rheology response of aqueous cellulose solutions was characterized using dripping-onto-substrate (DoS) rheometry. The experimental setup includes a dispensing and imaging system, as shown in Figure 1c. A finite volume of fluid is dispensed through a stainless-steel nozzle and is deposited on a clean glass substrate at a height H below the nozzle. The nozzle radius is kept constant for all experiments for HEC solutions with outer diameter, $D_0 = 2R_0$ = 1.27 mm and an inner diameter, D_i = 0.838 mm, whereas for hmHEC solutions, $2R_0$ = 2.108 mm and an inner diameter of D_i = 1.6 mm. The fluid is pumped at a low and fixed flow rate (Q = 0.02 mL/min) and an aspect ratio of $H/D_0 \approx 3$. The imaging system includes a light source, diffuser, and high-speed camera (Fastcam SA3 with a Nikkor 3.1× zoom (18−25 mm) lens). A macro lens is also used to improve magnification at the frame rates used (8000−25 000 frames/s). The DoS videos are analyzed with ImageJ and specially written MATLAB codes to determine the minimum neck radius as a function of time.
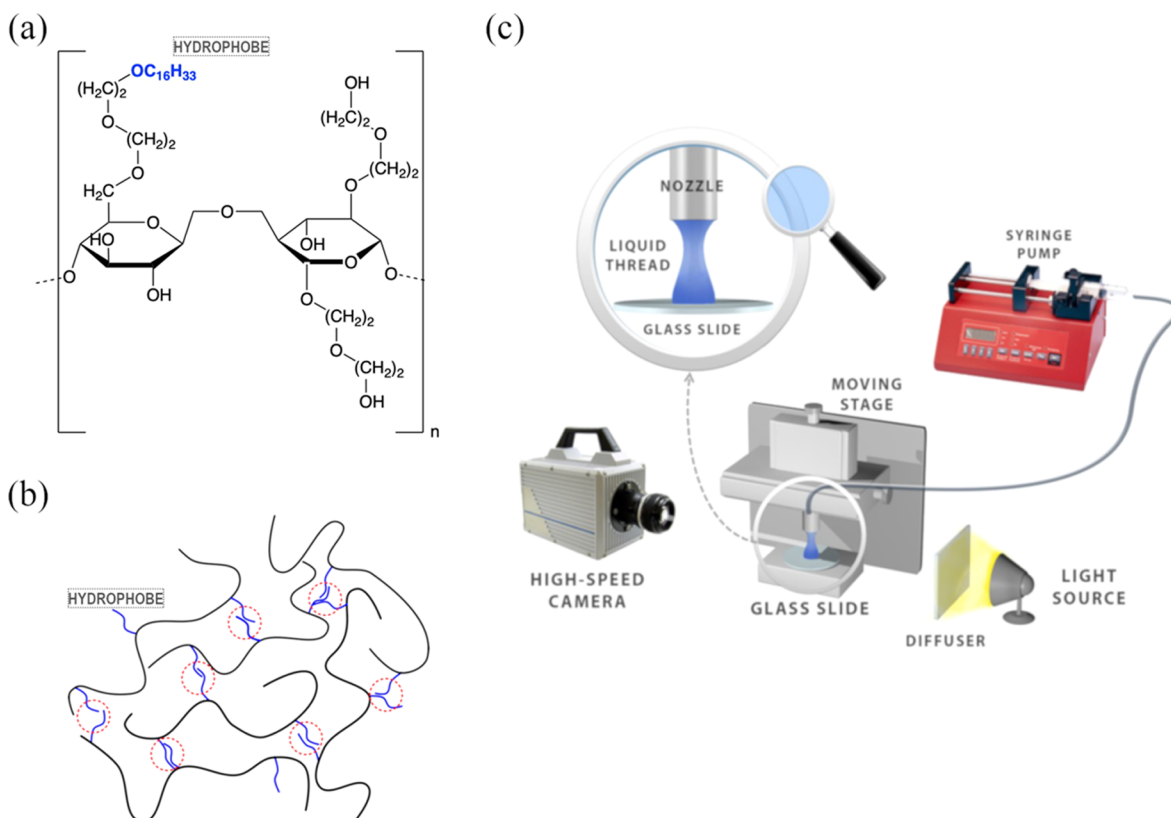
Figure 1. Schematics showing the structure of hydrophobically modified hydroxyethyl cellulose (hmHEC) and dripping-onto-substrate (DoS) rheometry setup. (a) Cellulose ether hmHEC incorporates hydroxyethyl groups with M.S.= 2.5 and includes hydrophobic stickers (cetyl group or C-16) with M.S. = 0.01. (b) Schematic showing association mediated by hydrophobic stickers among hmHEC chains. (c) DoS rheometry involved the visualization and analysis of thinning liquid neck (zoomed-in image). An unstable liquid bridge is created by releasing a finite fluid volume onto a fixed substrate using a dispensing system that includes a syringe pump connected to a nozzle. The imaging system consists of a high-speed camera (with magnification lenses) and a light source with a diffuser.

DoS rheometry relies on the analysis of pinching dynamics using radius evolution data, in analogy with other capillarity-based techniques, like capillary break-up extensional rheometer (CaBER) and other devices that rely on necks formed by applying step-strain to liquid bridges confined between two parallel plates,[53,61–64,69,76–82] or dripping,[83–85] or jetting-based rheometry.[5,57,86–91] Analysis of pinching dynamics is increasingly preferred for evaluating extensional rheology response at rates and conditions similar to drop formation and coating processes. However, as the commercially available CaBER (and its variants) analyzes the pinching dynamics of the neck created by applying step-strain to liquid confined between two parallel plates, two well-documented problems arise. (i) For low viscosity (η < 50 mPa·s), or low elasticity (relaxation time, λ < 1 ms) fluids, pinching occurs before initial step-strain deformation is completed.[69,80] (ii) The magnitude and time of step-strain influence the pinching dynamics for microstructured materials like gels, micellar solutions, and polymer–particle mixtures.[81,92,93] Detailed accounts of the utility and application of DoS rheometry protocols for measurements of capillarity-driven pinching dynamics and extensional rheology response for a range of complex fluids are already published. The list includes polymer and polyelectrolyte solutions,[23–30,94–100] inks,[25,101] micellar solutions,[25,102–104] and industrial fluids with yield stress and/or power law rheology[25] including particle suspensions, Carbopol solutions, emulsions, foods (mayonnaise and ketchup), and cosmetics like nail lacquer formulations.[105] The specific challenges that arise for extensional rheology characterization of polysaccharides are explored in great detail in the recent studies by Dinic and Sharma,[29,30] and therefore, we restrict the discussion here primarily for investigating the influence of stickers.

Pinching Dynamics: Neck Shapes and Radius Evolution Profiles. Table 2 summarizes and lists typical neck shapes and radius evolution profiles associated with capillarity-driven pinching flows of Newtonian and non-Newtonian fluids. The local balance of capillarity, inertia, and viscous stresses determine the pinching dynamics for Newtonian fluids,[58–60] and additional contributions from rate-dependent viscosity and elastic stresses determine the pinching dynamics for many complex fluids.[25,30,53,60] Low-viscosity Newtonian solvents like water exhibit a single conical neck, and radius evolution displays inertiocapillary (IC) response.[59,106–109] In contrast, higher viscosity Newtonian fluids like glycerol exhibit a slender, cylindrical neck that exhibits viscocapillary (VC) pinching dynamics if Ohnesorge number, $Oh = t_{VC}/t_R$ > 1.[108–111] Here, $Oh = \eta/\sqrt{\rho\sigma R_0}$ represents a dimensionless viscosity for a fluid with viscosity, η, density, ρ, and surface tension, σ. Non-Newtonian formulations that show strong shear-thinning response exhibit power law as pinching behavior and the neck pinches by forming two cones for power law index, n < 0.66, whereas for n > 0.66, pinching of slender, cylindrical necks is observed.[25,53,112–116]
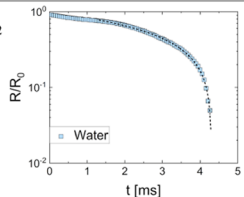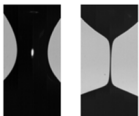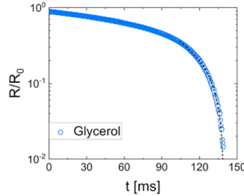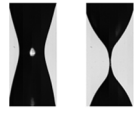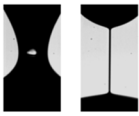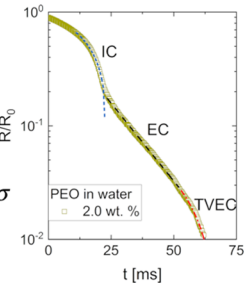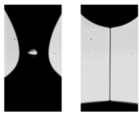
The addition of long, flexible polymers leads to extra viscoelastic stresses, slowing down of pinching, and a delay in the pinch-off event, typically due to elastocapillary (EC) response, manifested with an exponential decay in radius.[23–30,62,76,89,116–118] Detailed discussion of pinching dynamics anticipated by different constituent models for non-Newtonian fluids can be found in collaborative papers and reviews by Yarin,[57,63,64,117] Renardy[114–116,119] and Mc-Kinley.[53,89,111,118] The modified expression listed in Table 2 (introduced by Dinic and Sharma[26]) allows accounting for the onset of EC at t_c, and the computation of the extensional relaxation time, λ_E, as well as an app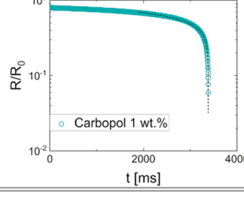arent extensional modulus, G_E.[23–26,29] In addition to EC response, finite extensibility effects[26,62–64,120] can sometimes result in a terminal viscoelastocapillary (TVEC) response with $R(t) \propto (t_f - t)/t_{TVEC}$, yielding the measurements of the steady,

Table 1. Published Measurements of Extensional Rheology Response of Associative Polymer Solutions

Authors (year)	M_w (kg/mol)	c (wt. %)	Technique	Remarks	Ref
Tan et al. (2000)	200	semidilute	opposed jets	bare vs sticky HASE: sticky shows extensional thinning	70
Patruyo et al. (2002)	300	varying	opposed jets and porous media	HEC vs hmHEC: the influence of SDS	38
González et al. (2005)	300	varying	opposed jets and porous media	xanthan gum and hmHEC primarily show strain-softening	37
Sharma et al. (2015)	240	semidilute	jetting-based (ROJER); microfluidic	EHEC vs hmEHEC; hmEHEC solutions exhibit extensional thinning	5

Table 2. Capillarity-Driven Pinching Dynamics, Characteristic Neck Shapes and Timescales[a]

Newtonian Low viscosity

Inertiocapillary (IC)

$$\frac{R(t)}{R_0} = X\left(\frac{\sigma}{\rho R_0^3}\right)^{1/3}(t_f - t)^{2/3}$$

$$0.4 \leq X \leq 0.8$$

$$t_R = \left(\rho R_0^3/\sigma\right)^{1/2}$$

$$Oh < 1 \quad Wi = 0$$

$$Ec = 0$$

Chen & Steen. *J. Fluid Mech.* (1997), Day, Hinch & Lister. *Phys. Rev. Lett.* (1998)
Eggers & Fontelos. *Singularities: Formation, Structure and Propagation* (2015), Dinic & Sharma. *Phys. Fluids* (2019)

Newtonian High viscosity

Viscocapillary (VC)

$$\frac{R(t)}{R_0} = \frac{(2X-1)}{6}\frac{\sigma}{\eta R_0}(t_f - t)$$

$$0.5324 \leq X \leq 1$$

$$t_{VC} = \eta R_0/\sigma$$

$$Oh > 1 \quad Wi = 0$$

$$Ec = 0$$

Papageorgiou. *Phys. Fluids* (1995), McKinley & Tripathi. *J. Rheol.* (2000)
Castrejon-Pita, Castrejon-Pita, Thete, Sambath, Hutchings, Hinch, Lister, Basaran. *PNAS* (2015)

Non-Newtonian Shear thinning

Power Law (PL)

$$\frac{R(t)}{R_0} = Y(t_f - t)^{n_c}$$

$$t_{PL} = Y^{-1/n_c}$$

$$Oh > 1$$

Renardy. *Rheol. Reviews* (2004), Doshi & Basaran. *Phys. Fluids* (2004)
McKinley. *Rheol. Reviews* (2005), Suryo & Basaran. *JNNFM* (2006), Dinic, Jimenez & Sharma. *Lab Chip* (2017)

Non-Newtonian Viscoelastic (VE)

Elastocapillary (EC)

$$\frac{R(t)}{R_0} \approx \left(\frac{G_E R_0}{2\sigma}\right)^{1/3}\exp\left(-\frac{t - t_c}{3\lambda_E}\right)$$

$$\lambda_E$$

$$\forall Oh \quad Wi = 2/3$$

$$De > 1 \quad Ec > 0$$

Entov & Yarin. *Fluid Dyn.* (1984), Yarin. *Free Liquid Jets and Films* (1993)
McKinley. *Rheol. Reviews* (2005), Clasen, Eggers, Fontelos, Li & McKinley. *J. Fluid Mech.* (2006), Dinic & Sharma. *PNAS* (2019)

Non-Newtonian Finitely Extensible VE

Terminal ViscoEC (TVEC)

$$\frac{R(t)}{R_0} = \frac{\sigma}{2R_0\eta_E^\infty}(t_f - t)$$

$$t_{TVEC} = 2R_0\eta_E^\infty/\sigma$$

$$\forall Oh \quad Wi > 1$$

$$De > 1 \quad Ec > 0$$

Renardy. *JNNFM* (1995, 2002), Entov & Hinch. *JNNFM* (1997)
Stelter, Bren, Yarin, Singh, Durst. *J. Rheol.* (2000, 2002), Fontelos & Li. *JNNFM*. (2004), Dinic & Sharma. *PNAS* (2019)

[a]The expressions derived from force balance in pinching neck, characteristic timescales, and the relevant dimensionless groups for low- and high-viscosity Newtonian fluids and non-Newtonian fluids with power law response and viscoelastic (elastocapillary (EC) or terminal viscoelastocapillary (TVEC)), respectively, are included together with selected references. The snapshots showing the characteristic neck shape and the radius evolution profiles were obtained by the coauthors using dripping-onto-substrate (DoS) rheometry.

terminal extensional viscosity η_E^∞ (where $Tr^\infty = \eta_E^\infty/\eta_0$ is defined as the terminal Trouton ratio and $t_{TVEC}/t_{VC} = Tr^\infty/3$) and the filament lifespan, t_f (or the overall pinch-off time).

RESULTS AND DISCUSSION

Steady Shear Viscosity Response of hmHEC Aqueous Solutions. Steady shear viscosity response as a function of shear rate appears nearly rate-independent for aqueous hmHEC solutions with the lowest concentrations shown ($c <$ 0.3 wt. %) in Figure 2a. However, the response for solutions with higher concentrations ($c >$ 0.4 wt. %) shows shear thinning. The onset of shear thinning shifts to a lower critical shear rate as the concentration of hmHEC increases. The rate-dependent variation in shear viscosity shown in Figure 2a,b (as

dotted lines) can be approximately captured by the four-parameter Cross model,[121] with the following expression

$$\eta = \eta_\infty + \frac{\eta_0 - \eta_\infty}{1 + (\lambda_s \dot{\gamma})^m} \tag{1}$$

Here, the shear relaxation time ($\lambda_s = 1/\dot{\gamma}_c$) is correlated with a critical shear rate, $\dot{\gamma}_c$, that characterizes the onset of shear-thinning response. The rate-independent zero shear viscosity, η_0, correlates with the size and the interactions of nearly unperturbed coils, whereas high shear-rate viscosity, η_∞, captures any modification in solvent dynamics. The exponent, m, quantifies the rate dependence of the viscosity. Though data sets in Figure 2a appear to show a pronounced shear thinning at high shear rates, Figure 2b shows that a few hmHEC
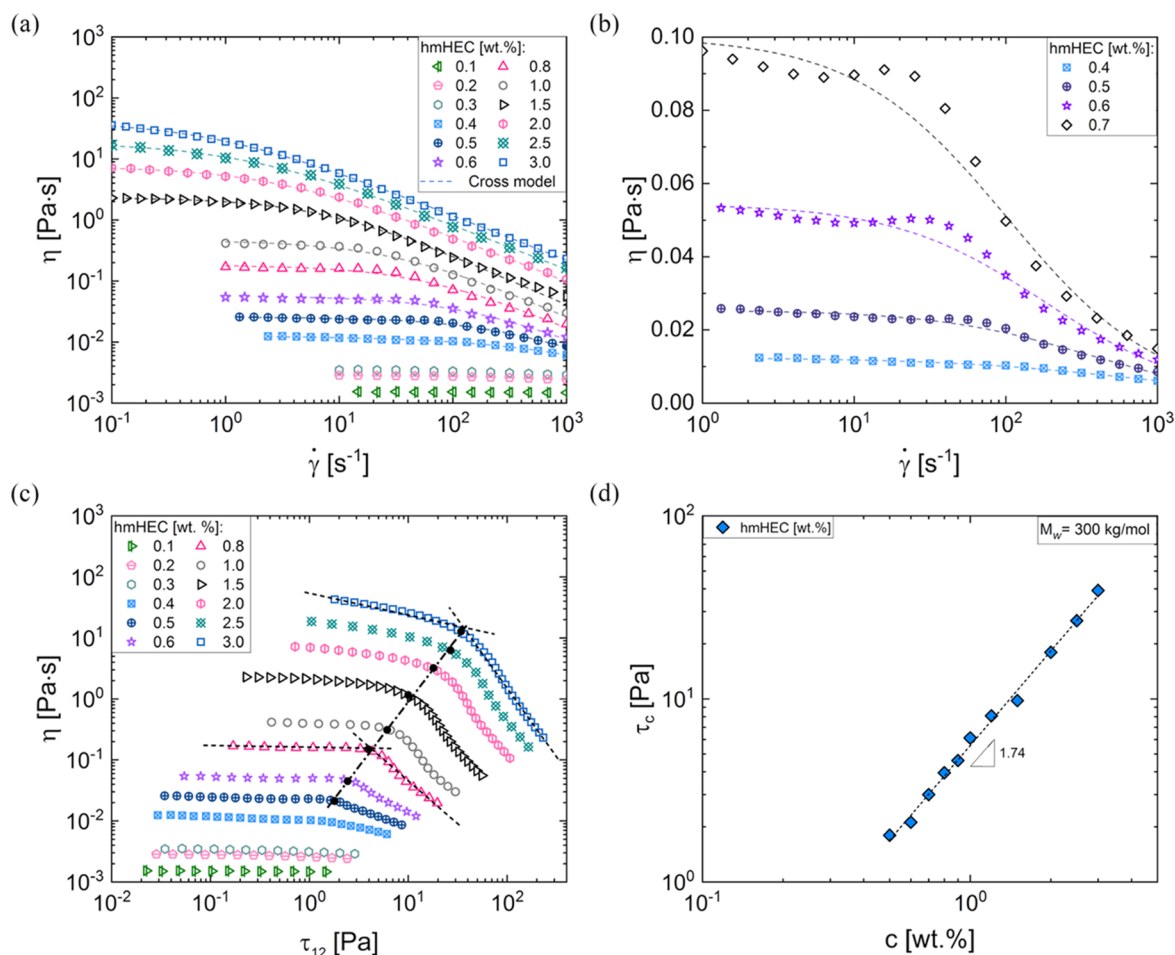
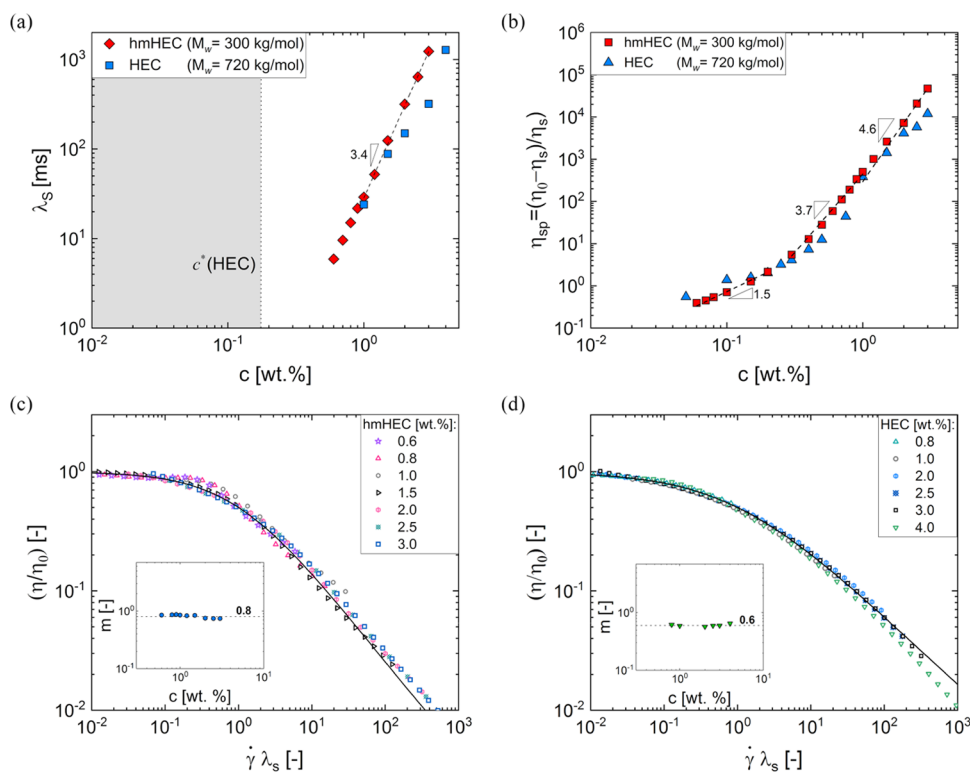**Figure 2.** Steady shear viscosity of aqueous solutions of hydrophobically modified hydroxyethyl cellulose (hmHEC). (a) Steady shear viscosity as a function of shear rate of aqueous solutions of sticky hmHEC (M_w = 300 kg/mol) exhibits a concentration-dependent increase and rate-dependent response with significant shear thinning at high shear rates as the concentration of hmHEC is increased. Dotted lines show Cross model fits to the viscosity data. (b) Shear viscosity plotted using linear ordinate values as a function of shear rate reveals slight shear thickening at median shear rates for the four concentrations included. (c) Shear viscosity as a function of shear stress, showing that a significant drop in viscosity occurs beyond some critical shear stress (τ_c). The locus of critical stress is shown with the dashed-dotted line. (d) Concentration-dependent increase in critical shear stress, τ_c, can be captured by a power law, $\tau_c \propto c^k$ with $k = 1.74$.

solutions (0.4 < c < 1.0 wt. %) exhibit mild but measurable shear thickening for intermediate shear rates. Similar mild shear thickening, reported before for aqueous solutions of multisticker associative polymers, including hmHEC,[32,122] was attributed to the shear-induced structuring of the transient network. Considerably more studies have probed shear thickening in telechelic associative polymers and attributed the mild increase in viscosity to the influence of the creation–destruction rate of hydrophobic associations and chain stretching and orientation in response to applied deformation fields.[123−132] The absolute enhancement in viscosity due to shear thickening (see Figure 2b) is relatively low in magnitude (note the ordinate values are on a linear scale) compared to the orders of magnitude change for particle suspensions.[2,133,134] Furthermore, as the mild thickening is manifested only for 0.4 < c < 1.0 wt. % hmHEC solutions, the Cross model provides a pragmatic description of rate-dependent viscosity illustrated in Figure 2b.

The steady shear viscosity data sets, shown in Figure 2a,b as a function of shear rate, $\dot{\gamma}$, are replotted as a function of stress, τ, in Figure 2c. Using stress as a control variable provides a better representation for understanding structural transitions,

especially the apparent yielding behavior displayed by many paint formulations.[135−139] Furthermore, many processing steps involve control over stress rather than shear rate, as also discussed in the reviews by Eley.[135,136] Figure 2c suggests that the viscosity drop can also be attributed to the shear-induced disruption of the associative network under the influence of an extra stretching force, or effective stress acting on stickers. Alternatively, the breakdown of the physical network structure at deformation rates that exceed the relaxation rate (primarily set by the shear-induced disassociation of stickers) results in a significant decrease in the viscosity at higher rates and larger exponent, m, for associative polymers. The viscosity value decreases substantially above a critical stress value, τ_c, computed using the intersection of dashed lines that fit viscosity changes at lower and higher stress, as illustrated in Figure 2c. The dashed lines show that the measured viscosity for c > 1 wt. % exhibits a weak stress dependency even for τ < τ_c, though more dramatic thinning is observed for τ > τ_c. The critical shear stress values, plotted in Figure 2d, display $\tau_c \propto c^k$ with $k = 1.74$, and measured values increase by 50 times as concentration increases from 0.3 to 3 wt. %. Aubry and Moan[52] had reported $\tau_c \propto c^{1.7}$ in the same range of scaled

Figure 3. Shear relaxation time, specific viscosity, and scaled shear viscosity curves of aqueous solutions of sticky hmHEC (M_w = 300 kg/mol) and bare HEC solutions (M_w = 720 kg/mol). (a) Shear relaxation time obtained from Cross model fits shows a concentration-dependent increase, $\lambda_s \propto c^k$, with an exponent, k = 3.4, for hmHEC solutions. Similar scaling is observed for HEC solutions when considering the concentrations deep into the entangled regime. (b) Specific viscosity as a function of concentration for aqueous hmHEC and HEC solutions reveals that entangled hmHEC solutions exhibit a stronger concentration dependence, $\eta_{sp} \propto c^k$, with k = 4.6 in comparison to k = 4.3 observed for entangled HEC solutions. The stronger exponent observed for the entangled regime and an additional regime at intermediate concentrations with exponent, k = 3.7, observed for hmHEC solutions can be attributed to the role played by hydrophobically associative stickers. (c) Universal scaled shear viscosity curve for hmHEC aqueous solutions obtained by scaling viscosity values with the corresponding zero shear viscosity values and multiplying shear rate with the corresponding λ_s values obtained using the Cross model fits. The inset shows that the exponent used in the Cross model exhibits roughly constant values of around m = 0.8. A similar approach was used to obtain the universal shear viscosity curve for the HEC solutions shown in (d), and the inset shows that the exponent is slightly lower and around m = 0.6.

concentration (c/c^*) for hydrophobically modified guar gum; Zhao and Chen[32] found $\tau_c \propto c^{1.62}$ for hmHEC (M_w = 550 kg/mol). In contrast, English et al.[125] reported a significantly higher value of k = 5 for a hydrophobically modified alkali-soluble emulsion (HASE) associative polymer. The drop in viscosity beyond critical stress does not occur as precipitously for the sticky hmHEC solutions as observed for solutions of telechelic hydrophobically modified urethane-ethoxylate (HEUR) associative polymers[127] or of HASEs that contain polyelectrolyte-like random copolymer backbone of methacrylic acid (MMA) and ethylacrylate (EA) together with pendant hydrophobic macromonomers (hydrophobically associating stickers).[140]

The values of apparent shear relaxation time, λ_s = $1/\dot{\gamma}_c$, extracted from Cross model fits, plotted in Figure 3a, for the aqueous hmHEC solutions have a higher magnitude and stronger concentration dependence ($\lambda_s \propto c^{3.4}$) than the HEC solutions ($\lambda \propto c^{2.4}$). For bare polymers including HEC solutions, the conformational anisotropy that arises in response to high deformation rates ($Wi = \lambda_s\dot{\gamma} > 1$) results in the shear-thinning response.[7−10,15,141] Here, the longest chain relaxation time, λ_s, for bare polymers depends on macromolecular dynamics. In contrast, for the solutions of multisticker associative polymers including aqueous hmHEC solutions, the strength and number of interchain and intrachain

associations govern the onset and extent of the rate-dependent response.[125,142]

Figure 3b shows the concentration-dependent change in specific viscosity, $\eta_{sp} = (\eta_0 - \eta_s)/\eta_s$, values computed using zero shear viscosity, η_0 values extracted using Cross model fits, and solvent viscosity (η_s = 8.9×10^{-4} Pa·s). Despite the higher molecular weight, at matched concentration, specific viscosity values measured for HEC solutions appear to compare well with the values obtained for hmHEC solutions. The critical overlap concentration, c^*, estimated as the concentration at which polymer contribution to solution viscosity equals solvent viscosity (or using η_{sp} = 1), is comparable at ∼0.1 wt. % for both HEC and hmHEC solutions. A slightly higher value of c^* = 0.17 wt. % is estimated from the change in slope of $\eta_{sp}-c$ plot yielding intrinsic viscosity, $[\eta] \approx 6$ dL/g, as also reported earlier.[29,30] However, for associative polymers, the presence of intrachain interactions can reduce effective coil sizes, whereas the formation of aggregates (micelles/clusters) can lead to a larger effective coil size.[1,34,143] In what follows, we chose not to plot measured quantities in terms of scaled concentration, c/c^* for hmHEC solutions, as the apparent intrinsic viscosity is not a measure of coil size, and c/c^* (or Berry number, $c[\eta]$) is not correlated with the contribution of individual coils or their interactions, unlike the case for bare chains.[33,34] Indeed, using Mark−Houwink−Sakurada relationship, $[\eta] = KM^a$ with a =

0.73 and $K = 4.1 \times 10^{-2}$ mL/g (see review by Clasen and Kulicke for discussion[20]), the estimated value for HEC (M_w = 720 kg/mol) is $[\eta]$ = 7.7 dL/g (c^* = 0.13 wt. %), whereas a bare HEC of lower M_w = 300 kg/mol is expected to have $[\eta]^{bare}$ = 4 dL/g (and higher c^{*bare} = 0.25 wt. %).

Specific viscosity of HEC solutions exhibits three distinct scaling regimes: $\eta_{sp} \propto c$ in dilute ($c < c^*$), $\eta_{sp} \propto c^2$ in the semidilute, unentangled ($c < c^* < c_e$), and $\eta_{sp} \propto c^{4.3}$ in the entangled ($c > c_e$) regime, beyond c_e = 0.5 wt. % (corresponds to $c_e/c^* \approx 3$), in agreement with the previous reports for HEC and other polysaccharides.[29,30,52,144] Specific viscosity of hmHEC solutions also exhibits three regimes: $\eta_{sp} \propto c^{1.5}$ (for $c^{*bare} < 0.25$ wt.%), $\eta_{sp} \propto c^{3.7}$ in the semidilute, unentangled ($c^{*bare} < c < c_e$), and $\eta_{sp} \propto c^{4.6}$ in the entangled ($c > c_e$) regime. The exponents observed appear to be similar to scaling exponents for $\eta_{sp} \propto c^k$ (ranging from k = 3.65−5) reported for hydrophobically modified polysaccharides and hydrophobically modified polyelectrolytes.[44,145,146] Extensive studies on solutions of HASE polymers that contain random copolymer backbone of methacrylic acid (MMA) and ethylacrylate (EA), together with pendant hydrophobic macromonomers (stickers), show weaker exponents ($k < 3$) if the solvent quality is decreased or if the sticker fraction is substantially lower,[143] but much stronger exponents ($k > 7$) can be observed in certain MAA:AA:sticker fractions.[125,147,148]

Scaling viscosity with zero shear viscosity and then plotting it as a function of shear Weissenberg number, $\lambda_s \dot{\gamma}$ results in a universal flow curve shown in Figure 3c,d. Such universal flow curves reveal that the dynamic modes of relaxation with similar concentration dependence govern the response for the entire range of deformation rates. Similar normalized flow curves can be obtained for other cellulose derivatives, listed and reviewed elsewhere.[20] The slight mismatch among the flow curves presented in Figure 3c for a few intermediate concentrations is due to a mild but measurable shear thickening effect. The values of exponent, m, obtained from the Cross model fits to the steady shear viscosity data as a function of concentration appear to be reasonably well-matched at $m \approx 0.8$ for hmHEC and lower value of $m \approx 0.6$ for HEC (see the insets for Figure 3c,d). The higher value of m for the aqueous hmHEC solutions is consistent with a higher degree of shear thinning observed for these associative polymer solutions.

Shear Viscosity and Shear Relaxation Time of Multisticker Associative Polymers. A significant drop in viscosity observed in Figure 2a−c occurs as stickers become increasingly ineffective at shear rates exceeding relaxation rate $(1/\lambda_s)$, depends on the sticker association−disassociation rate $(1/\lambda_{sad})$. The onset of shear thinning and the relaxation spectrum of associative polymer solutions are influenced by the sticker association−disassociation time, λ_{sad}, and polymer chain and aggregate (micelle/cluster) dynamics. The physical associations between hydrophobically modified chains break and form continuously even in the quiescent state under ambient thermal fluctuations, with an intrinsic, sticker association−disassociation time, $\lambda_{i,sad} \approx \Omega^{-1} \exp(\Delta G_{BE}/k_B T)$, computed using arguments put forth by Bell,[149] Tanaka and Edwards,[150] and others.[151−153] Here, $\lambda_{i,sad}$ depends on the activation barrier for disassociation or pairwise binding energy, $\Delta G_{BE} \cong 0.98 n_{CH_2} k_B T$, which is determined by the number of carbon atoms per sticker, n_{CH_2}, and is presumed to be nearly independent of the length of the backbone chain.[124,150,153−155] For hmHEC (C-16) with 16 methyl groups in hydrophobic

sticker, under quiescent state, $\lambda_{i,sad} \approx 6.5$ ms using the mean value of prefactor, $\Omega \approx 10^8 - 10^{10}$ Hz for thermal vibration frequency. Thus, the values of λ_s shown in Figure 3a are up to 2 orders of magnitude larger than $\lambda_{i,sad}$. An additional energy barrier, ΔG_{MS}, arises in multisticker polymers due to the chain's inability to relax even after one pair of stickers disassociates.[2,7−9] This extra energetic penalty, which increases with concentration, effectively increases the time spent by stickers in close vicinity of each other, leading to the formation of polydisperse clusters within the material.[9] Finally, under a nonlinear or strong external deformation characterized by force f, the magnitude of sticker association−disassociation time, $\lambda_{sad} \approx \Omega^{-1} \exp((\Delta G_{BE} + \Delta G_{MS} - fb)/k_B T)$, itself changes.[12,149,151−153] Thus, the combination of associations and clustering leads to a substantial increase in relaxation time as shown in Figure 3a, effectively providing sticky polymer of lower molecular weight (hmHEC, M_w = 300 kg/mol) with a similar onset of shear thinning as a higher M_w bare polymer (HEC, M_w = 720 kg/mol) at matched concentration.

According to transient network models,[2,15,141,150,154−156] the shear relaxation time of multisticker associative polymers can be described using the sticky Rouse model for unentangled, and the sticky reptation model for entangled solutions. The Rouse relaxation time, $\lambda_R = \lambda_0 N_K^2$, for a bare chain with Kuhn length, b_K, depends linearly on bead relaxation time, $\lambda_0 \approx \eta_s b_K^3/k_B T$ and quadratically on molecular weight or the number of Kuhn segments, N_K. Likewise, the sticky Rouse relaxation time, $\lambda_{SR} = \lambda_{sad} N_K^2/N_{KS}^2 = \lambda_{sad} f^2$, depends linearly on the sticker association−disassociation time, λ_{sad}, and quadratically on the number of stickers, estimated to be f = 11 by assuming the degree of polymerization = 1100 (and MS for C-16 stickers is 0.01). Here, the number of Kuhn segments between stickers is N_{KS}, and the disassociation events are considered independent events. The Rouse relaxation time estimated for bare HEC (M_w = 720 kg/mol) in water using N_K = 70 and Kuhn length, b_K = 20 nm was previously reported to be λ_R = 0.09 ms, with a slightly lower value Zimm relaxation time, λ_Z = 0.07 ms.[29] The corresponding estimate of the Rouse relaxation for bare HEC with the same chain length as hmHEC (M_w = 3.0 × 10^5 g/mol) is λ_R = 0.015 ms, which is considerably shorter than the estimated $\lambda_{i,sad} \approx 6.5$ ms or $\lambda_{i,SR} \approx 787$ ms and the measured λ_s (see Figure 3a) implying the relaxation dynamics are determined by the lifetime of transient bonds. In semidilute, unentangled solutions of bare polymers, the dynamics follow a Rouse−Zimm relaxation such that the Rouse chain with N_K/g blobs and blob relaxation time estimated using Zimm chain with g segments, leading to $\lambda_{RZ} \propto \lambda_0 N_K^2 \phi^{0.31}$ in good solvent and $\lambda_{RZ} \propto \lambda_0 N_K^2 \phi^1$ in θ solvent.

We find that the concentration-dependent increase in specific viscosity can be rationalized using the theoretical model advanced by Rubinstein and Semenov[8,9] for solutions of strongly associative polymers containing $N = N_K$ segment chains with f associating groups separated with the number of segments $l = N_{KS}$, with $f \gg 1$; $l \gg 1$ and $N = fl$. A mean-field threshold volume fraction $\phi_{pg} \approx l^{-0.77} f^{-0.63}$ for physical gelation is predicted in semidilute solutions by counting only the fraction of stickers involved in the interchain association. As increasing the number density of chains results in an increase in the fraction of stickers in interchain junctions, all pairings become interchain above a sticky overlap volume fraction $\phi_s \approx l^{-0.77}$. We rewrite the two expressions as $\phi_{pg}/\phi^* = c_{pg}/c^* \approx f^{0.14}$ and $\phi_s/\phi^* = c_s/c^* \approx f^{0.77}$, respectively, for polymers dispersed in a good solvent. For hmHEC solutions with f = 11,
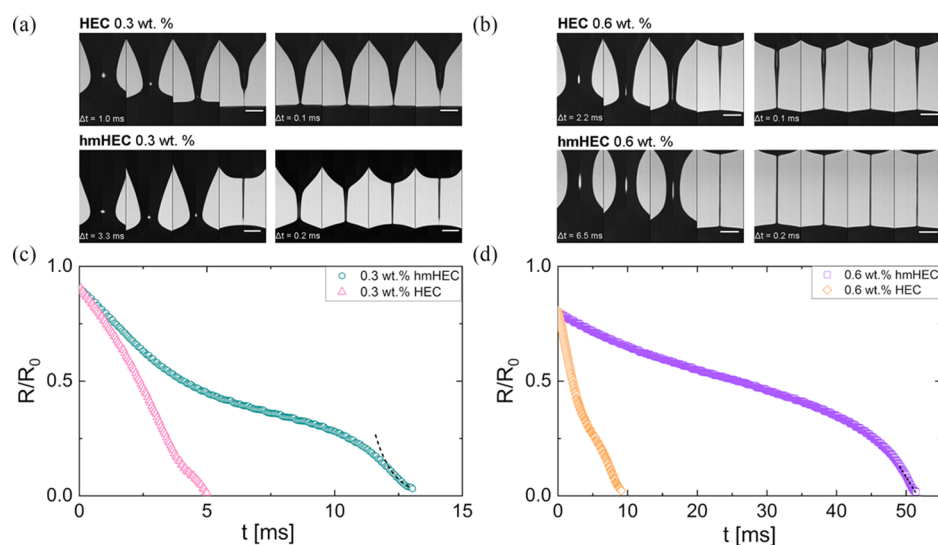
Figure 4. Neck shape and radius evolution of sticky vs bare polymers. (a) First four snapshots that are $\Delta t = 1$ ms apart show the shape evolution of the pinching neck for 0.3 wt. % HEC solution, with a single sharp cone, characteristic of the inertiocapillary response. The second set of four snapshots that are $\Delta t = 0.1$ ms apart and focus on the late stage before the pinch-off event show that the appearance of a filament in the last stage increases filament lifespan. (b) Neck shape for 0.6 wt. % with $\Delta t = 2.2$ ms shows the formation of slender, cylindrical filament, highlighted in late stage by snapshots $\Delta t = 0.1$ ms apart. The corresponding trends are emulated in hmHEC neck shapes. However, as filament lifespan is longer for hmHEC solutions, larger time steps of $\Delta t = 3.3$ ms and $\Delta t = 6.5$ ms are used for $c = 0.3$ wt. % and $c = 0.6$ wt. %, respectively. The late-stage evolution is also shown with longer $\Delta t = 0.2$ ms. (c) Comparison of radius evolution data for 0.3 wt. % HEC and hmHEC solutions shown on the linear–linear plot. (d) Radius evolution data for 0.6 wt. % for HEC and hmHEC solutions. For matched concentrations, the bare polymer HEC with a higher $M_w = 720$ kg/mol than sticky hmHEC ($M_w = 300$ kg/mol) shows comparable shear viscosity values but exhibits a large contrast in the neck shape, radius evolution, and filament lifespan.

this scaling analysis gives a gelation concentration $c_{pg}/c^* \approx 1.4$ or $c_{pg} = 0.35$ wt. % and a critical sticky overlap concentration $c_s/c^* \approx 6.3$ or $c_s \approx 1.6$ wt. %. The onset of shear thinning (see Figure 2a) occurs above c_{pg}, and the absence of well-defined stress-independent or rate-independent shear viscosity (in the low shear rate limit) occurs approximately above c_s. The concentration-dependent variation in specific viscosity shown in Figure 3b for hmHEC solutions displays similar critical values. Above c_{pg}, chains relax via multiple breaking and reforming of reversible bonds, acting as effective friction centers (sticky points) within the sticky Rouse model. As a result, the viscosity increases rapidly for multisticker chains when the timescale of disassociation is longer than the relaxation time of a strand between two stickers. Although specific viscosity exhibits change in concentration-dependent exponent from $k = 3.7$ to 4.6, for hmHEC solutions, the relaxation time seems to show $\lambda_s \propto c^{3.4}$, for all nondilute hmHEC solutions. The exponent of $k = 3.4$ displayed by sticky hmHEC solutions is far stronger than the exponent $k = 0.31$ (or 1) expected for semidilute, unentangled, and $k = 1.6$ (or 7/3) anticipated for semidilute, entangled solutions of bare polymers in a good (or θ) solvent. However, HEC solutions display $\lambda_s \propto c^{2.4}$ for semidilute, entangled solutions with exponent, $k = 2.4$, close to the value expected in θ solvent. In contrast, the variation in zero shear viscosity and relaxation time in dilute solutions is consistent with the expectations for polymers dissolved in a good solvent,[29,30] attributed to the progressive screening of excluded volume interactions with increased concentration.

Pinching Dynamics and Extensional Rheology of Aqueous Solutions of Sticky Polymers. The neck shape evolution over time and pinching dynamics of hmHEC and HEC solutions were characterized using dripping-onto-substrate (DoS) rheometry protocols. Figure 4a,b contrasts

the image sequences for two sets of data obtained at matched concentrations of HEC and hmHEC. Significantly shorter filament lifespan is obtained for the solutions of HEC as contrasted against hmHEC, even though the solutions have comparable shear viscosity, and bare chain polymer HEC has a higher molecular weight. The first four snapshots in each sequence show the entire evolution of the pinching neck by including the first snapshot with a nearly matched initial (scaled) neck radius and the last snapshot before the pinch-off event. The second set of four images with shorter time steps ($\Delta t = 0.1$ ms for HEC and $\Delta t = 0.2$ ms for hmHEC) is included to compare and contrast the neck shape variation before pinch-off. The image sequences shown for 0.3 wt. % HEC and hmHEC solutions reveal the presence of a conical neck shape reminiscent of inertiocapillary response. In contrast, the neck shapes for 0.6 wt. % solutions display a slender cylindrical neck, as shown in Figure 4b. However, a detailed observation of the neck shape in snapshots for 0.3 wt. % before the pinch-off event reveals a cylindrical filament emerges in the late stage. Likewise, the analysis of the radius evolution data displayed on a linear–linear scale reveals a transition to a distinct regime (see Figure 4a,c) that delays the pinch-off event compared to a Newtonian fluid. The dotted lines shown in Figure 4c are respective fits: an elastocapillary (EC) response for 0.3 wt. % HEC solution and the terminal viscoelastocapillary (TVEC) for 0.3 wt.% hmHEC solution (Figure 4c). The last regime is fit by EC and TVEC, respectively, for 0.6 wt. % HEC and hmHEC solutions, as shown in Figure 4d. Similar relatively short-lived elastocapillary (EC)/finite extensibility (TVEC) regions were observed for unentangled solutions of lower extensibility polyelectrolytes like polystyrene sulfonate (NaPSS) solutions and sodium carboxymethylcellulose (NaCMC).[27,28]
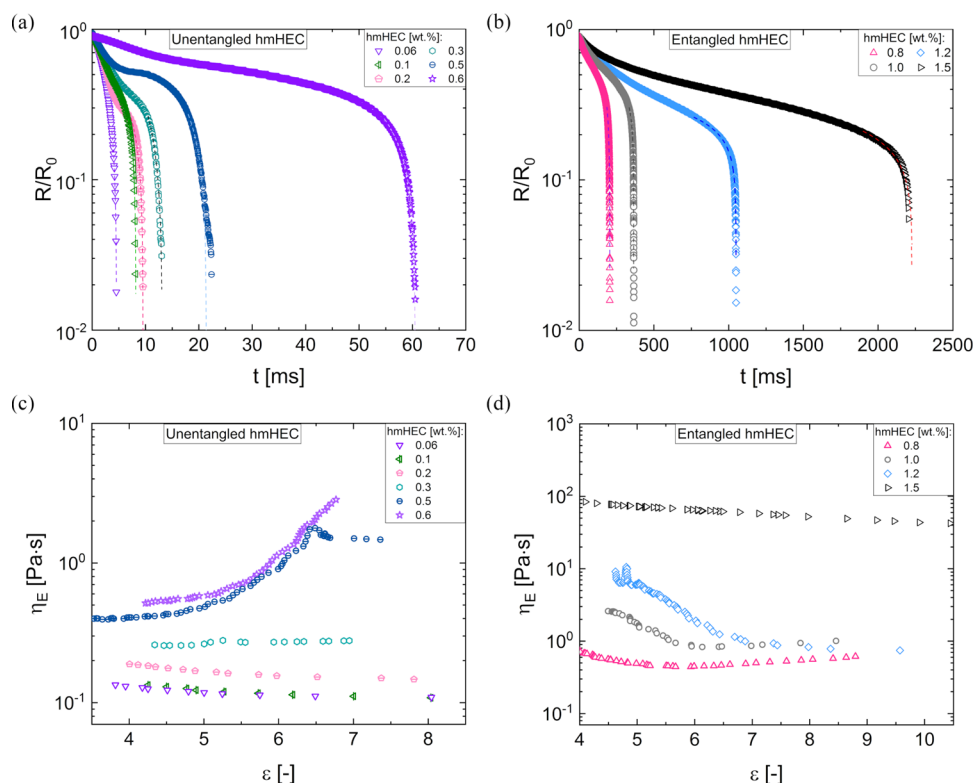
Figure 5. Filament radius evolution as a function of time for aqueous solutions and extensional viscosity of hmHEC solutions (M_w = 300 kg/mol). Radius evolution for (a) unentangled and (b) entangled hmHEC solutions. Dotted lines show the power law fit, though closer inspection reveals viscoelastic effects in the last stage before the pinch-off event. (c) Transient extensional viscosity as a function of strain for the lowest three (dilute) hmHEC solutions shows nearly constant terminal, steady-state values. In contrast, unentangled semidilute solutions show strain hardening at intermediate strains. (d) Transient extensional viscosity as a function of strain for entangled solutions (c > 1 wt. %) shows strain-softening.

Figure 5a presents the radius evolution data for a broader range of unentangled hmHEC solutions on a semilog plot using a logarithmic ordinate. Inertiocapillary dynamics, without any hint of viscoelastic stresses, are observed for c = 0.06 wt. % (dilute) hmHEC solution. In contrast, the radius evolution data for semidilute, unentangled solutions ($c^{*bare} < c < c_e$) display a relatively slow pinching rate in an initial regime, followed by a dramatic decrease in radius within a short time span in the second regime captured by terminal viscoelasto-capillary (TVEC) response. The radius evolution data for entangled hmHEC solutions in Figure 5b show a power law response before the manifestation of a short TVEC region, similar to the power law response detailed by Dinic and Sharma for entangled HEC solutions.[30]

Following the standard practice for extensional rheology characterization using capillarity-driven pinching flows,[26,29,30,53,69] we first show η_E as a function of Hencky strain, $\varepsilon = 2\ln(R_0/R(t))$, in Figure 5c,d for unentangled and entangled hmHEC solutions, respectively. The apparent extensional viscosity, $\eta_E = \eta_E^+(t,\dot{\varepsilon})$, of polymer solutions is computed from the radius evolution data using the extension rate, $\dot{\varepsilon} = -2\dot{R}(t)/R(t)$, and the expression, $\eta_E\dot{\varepsilon}(t) = \sigma/R(t)$, resulting from the balance between extensional stress and capillary stress determined by the ratio of surface tension, σ, to neck radius. The apparent extensional viscosity increases with concentration for dilute solutions (c = 0.06−0.3 wt. % in Figure 5c), showing a hint of strain hardening at low strains and nearly strain (and strain-rate) independent regime at the highest strain. In contrast, a strong strain hardening can be observed for the semidilute, unentangled 0.5 and 0.6 wt. %

hmHEC solutions before finite extensibility effects manifest. On increasing concentration further and deeper into the entangled regime, as shown in Figure 5d, the extensional viscosity exhibits strain-softening response at intermediate strains before displaying the finite extensibility regime with a constant, steady, terminal extensional viscosity.

The transient extensional viscosity responses of hmHEC and HEC solutions are contrasted in Figure 6a,b, respectively, as a function of extensional rate, $\dot{\varepsilon}$. For the lowest concentration (0.3 wt. %) shown, terminal, steady values are reached at $\dot{\varepsilon}$ > 10^3 s^{-1} for both solutions. In contrast, even though η_E vs ε plots (Figure 5c) show strain hardening followed by finite extensibility for unentangled 0.5 and 0.6 wt. % hmHEC solutions, the corresponding vs extensional rate curve bends backwards in Figure 6a due to the change slope in radius evolution plots (see Figure 5a) contributed by the influence of transient junctions. However, extensional viscosity responses are strikingly different for entangled solutions: HEC solutions exhibit nearly rate-independent viscosity, whereas associative hmHEC solutions show extensional thinning, followed by the regime with steady, terminal extensional viscosity, η_E^∞. For example, 1 wt. % solutions exhibit a higher value of η_E^∞, leading to the higher value of terminal Trouton ratio, $Tr^\infty = \eta_E^\infty/\eta_0$, for HEC solutions ($Tr^\infty \approx 11$ in contrast with $Tr^\infty \approx 0.8$ obtained for the hmHEC solution), even though extensional viscosity values are comparable at lower deformation rates.

The η_E^∞ and Tr^∞ values shown in Figure 6c,d, appear to be comparable for the sticky and bare polymer solutions up to 0.5 wt. %. However, η_E^∞ values for HEC solutions exhibit a significant increase for c > 0.5 wt. % due to the role played by
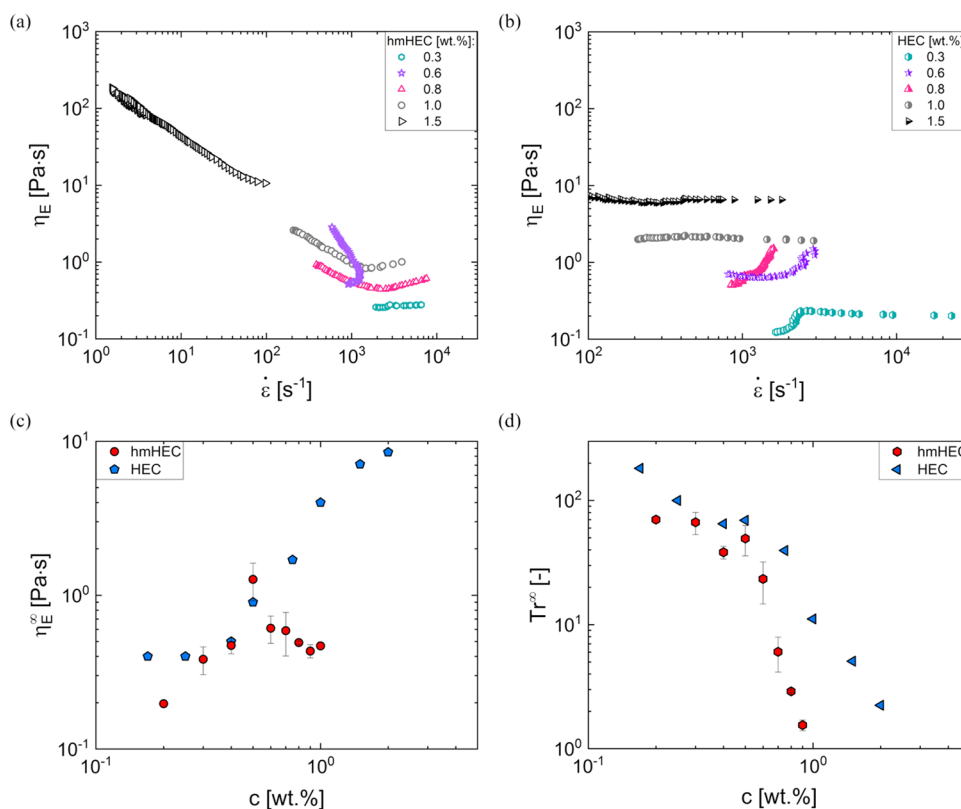
Figure 6. Contrasting variation in rate-dependent extensional viscosity. Extensional viscosity as a function of extension rate for the aqueous solutions of (a) sticky hmHEC (M_w = 300 kg/mol) and (b) bare HEC (M_w = 720 kg/mol). Extensional viscosity as a function of strain rate for unentangled hmHEC solutions also shows the nearly rate-independent plateau at deformation rates exceeding 10^4 s^{-1}. The transient networks formed by association and clustering are destroyed in strong extensional flows. (c) Steady, terminal extensional viscosity extracted from TVEC fits shows decreasing values for high hmHEC concentrations contrasted with increasing extensional viscosity for HEC solutions. (d) Terminal Trouton ratios are contrasted for aqueous hmHEC and HEC solutions. A sharper decrease is observed for associative polymer (hmHEC) solutions.

entanglements. In contrast, the destruction of transient bonds and disruption of the transient network lead to lower η_E^∞ values for hmHEC solutions consistent with the lower molecular weight than HEC. Sharma et al. showed that semidilute solutions of ethylhydroxyethyl cellulose (EHEC) exhibit extensional thickening in steady-state measurements of flow-induced birefringence and excess pressure drop across an extensional stagnation point flow using a cross-slot extensional rheometer, whereas solutions of its hydrophobically modified analogue (hmEHEC) exhibit extensional thinning.[5] Likewise, Tan et al. also reported extensional thinning for HASE polymers using the opposed jet technique,[70] though inertial effects influence the accuracy of these measurements.[157] Extensional thinning observed for hmHEC solutions arises due to the disruption of the transient network, especially at large extension rates that exceed both relaxation time and the sticker association−disassociation time. Though extensional thinning typically arises in structured fluids that exhibit shear-thinning behavior, it is also observed for nondilute polymer solutions in experiments[158−161] and simulations.[65,161,162] In such cases, the extensional thinning can be described using constitutive models like the Wiest model[163] and the Primitive Chain Network model[164,165] that incorporate finite extensibility along with anisotropic hydrodynamic drag.[163−167]

In addition to the measurement of extensional rheology response, the analysis of radius evolution data provides additional parameters (see Table 3 and Figure 7), including extensional power law index (n_e) and power law timescale (t_{PL})

obtained from the power law region, and filament lifespan (t_f) and η_E^∞ from the TVEC response. Table 3 also shows the three parameters, including zero shear viscosity (η_0), exponent (m), and apparent shear relaxation time ($\dot\gamma$) obtained by fitting the Cross model to the steady shear viscosity data (see Figure 2). Even though zero shear viscosity values are nearly matched and HEC solutions have higher molecular weight and higher terminal viscosity, the delayed pinch-off for the sticky polymer illustrates the possibility of an increase in frequency and duration of associations for the mildly stretched chains in the semidilute regime.

The extensional power law exponent, n_e, determined by fitting $R(t)/R_0 = Y(t_f - t)^{n_e}$ to the radius evolution data, exhibits a lower magnitude and a weaker concentration-dependent decrease for hmHEC solutions, as shown in Figure 7a. The values of Cross model exponent, m, tabulated in Table 3 and obtained by fitting the shear viscosity data in Figure 2 is related to the power law exponent, n, by $n = 1 - m$. The hmHEC solutions display distinct shear and extensional power law exponents, n and n_e, respectively. Theoretical studies based on the power law model $\tau = K\dot\gamma^n$ for rate-dependent shear viscosity predict $R(t)/R_0 = Y(t_f - t)^n$ or predict $n = n_e$, thus anticipating that the same exponent governs shear and extensional thinning behavior as characterized in torsional shear rheometry and capillarity-based extensional rheometry.[25,53,112,113,168] For $n \geq 0.6$, $Y = \Phi(n)\sigma/K = t_{PL}^{-n}$, where the constant $\Phi(n)$ is determined numerically, the constant K is called consistency, and $t_{PL} = Y^{-1/n_e}$ is used to compute a

Table 3. Concentration-Dependent Variation in Parameters Characterizing the Shear Rheology, Pinching Dynamics, and Extensional Rheology Response of the Aqueous hmHEC Solutions

c (wt. %)	η_0 (Pa·s)	m	λ_s (ms)	Oh	n_e	t_{PL} (ms)	t_f (ms)	η_E^∞ (Pa·s)	Tr^∞
0.2	0.0028			0.01	0.67		9.6	0.2	70
0.3	0.0058			0.03	0.50	35	13	0.4	67
0.4	0.012			0.06	0.65	22	25	0.5	38
0.5	0.026			0.12	0.85	17	63	1.3	49
0.6	0.053	0.85	5.9	0.2	0.67	84	67	0.6	23
0.8	0.17	0.86	15	0.8	0.40	306	168	0.5	2.9
0.9	0.28	0.87	22	1.3	0.35	535	267	0.4	1.5
1.0	0.45	0.85	29	2.1	0.34	1060	386	0.5	1.0
1.2	0.89	0.83	52	4.1	0.32	18 964	1049	1.0	1.1
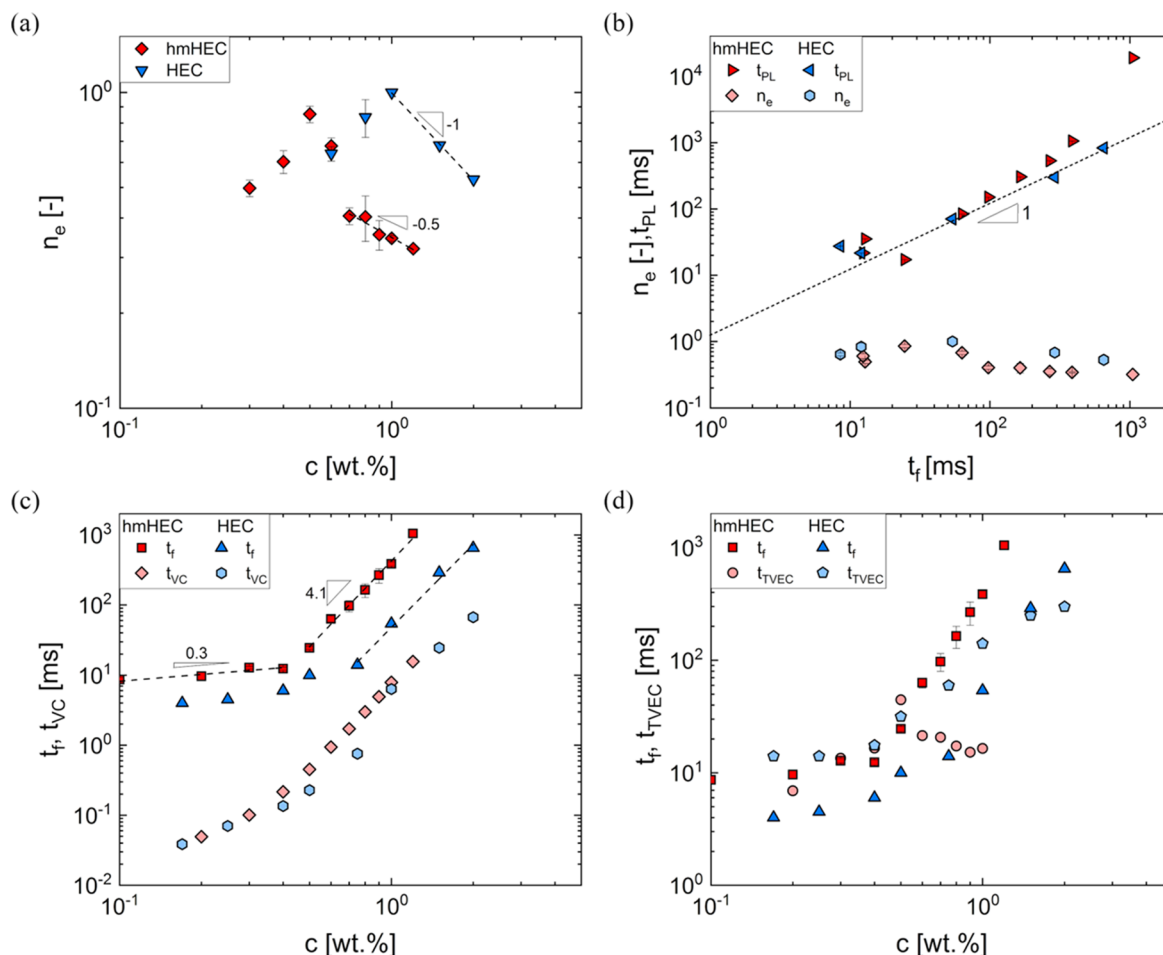
Figure 7. Parameters obtained from radius evolution data for aqueous solutions of sticky hmHEC (M_w = 300 kg/mol) contrasted against bare HEC solutions (M_w = 720 kg/mol). (a) Extensional power law exponent, n_e, extracted from radius evolution fits exhibit decreasing values at high concentrations with different scalings for both hmHEC and HEC solutions. (b) Extensional power law exponent, n_e, and The characteristic power law time, t_{PL}, extracted from radius evolution fits, scales linearly with filament lifespan, t_f for both hmHEC and HEC solutions. In contrast,, n_e values seem to be uncorrelated with t_f. (c) Comparison of the filament lifespan, t_f, and the estimated viscocapillary time, t_{VC}. Filament lifespan, t_f, sharply increases for hmHEC solutions at concentrations beyond 0.5 wt. %. Similar scaling is observed for HEC solutions. (d) Two timescales obtained by fitting radius evolution before pinch-off with the expression for terminal viscoelastocapillary pinching are compared here. The magnitudes of filament lifespan, t_f, and terminal viscoelastocapillary time, t_{TVEC}, in the low concentration regime for hmHEC solutions and in the high concentration limit for entangled HEC solutions appear comparable.

characteristic timescale.[25,53,112,113,168] Furthermore, such simulations anticipate the neck shape with two cones for $n < 0.67$ and a slender, cylindrical neck for $n > 0.67$ values.[25,112,168] The formation of two cones is not observed in our experiments even if $n < 0.6$ captures the shear-thinning response measured in torsional rheometry. Previous studies attribute this disagreement between n_e (extensional) and n (shear) to the influence

of deformation history and flow-type sensitivity of microstructural transitions of highly structured complex fluids.[25,30,105,169−173] Figure 7b shows that the values of t_{PL} extracted from power law fits are linearly correlated with the filament lifespan, t_f, even though n_e values seem uncorrelated with t_f.

Figure 7c contrasts the filament lifespan for HEC and hmHEC solutions. For hmHEC solutions, the filament lifespan shows a weak concentration-dependent increase with $t_f \propto c^{0.3}$ for $c < 0.4$ wt. % (approximately for $c < c_{pg}$) and a much stronger, $t_f \propto c^{4.1}$, dependence for higher concentrations. Also plotted in Figure 7c are the nearly matched values of viscocapillary time, $t_{VC} = \eta_0 R_0/\sigma$, for the aqueous solutions of the bare and the sticky polymer. The variation in t_{VC} is set primarily by the concentration-dependent change in zero shear viscosity as the characteristic size (nozzle radius) is matched and surface tension values are nearly matched in systems explored here. Comparison of t_{VC} and t_f shows that the knowledge of η_0 (and more generally shear rheology response) cannot be used to anticipate the magnitude and the concentration-dependent variation of filament lifespan. The disagreement is most stark for lower concentrations in semidilute HEC and hmHEC solutions.

However, Figure 7d shows that t_{TVEC} and t_f values are nearly matched below gelation concentration, $c_{pg} = 0.35$ wt. %, for hmHEC solutions. However, for $c > c_{pg}$, the filament lifespan, t_f of hmHEC solutions is influenced primarily by the initial kinematics governed by power law pinching behavior, whereas the viscoelastocapillary time, t_{TVEC}, decreases mirroring the change in terminal extensional viscosity, η_E^∞. In contrast, for HEC solutions, even though the magnitude of t_{TVEC} exceeds t_f values measured in the unentangled region, the values compare rather well in the highest concentrations observed. The close comparison in Figure 7c,d highlights how enhancement in the effective viscosity in response to extensional flows within pinching necks modulates deformation rates and timescales in processing operations involving drop formation or liquid transfer to substrates.

Recently, Dinic and Sharma showed that the chemistry-dependent contrast in macromolecular dynamics and extensional rheology response could be characterized a priori in terms of three ratios: contour length to Kuhn length (flexibility), contour length to unperturbed coil size (extensibility), and packing length to Kuhn length (a parameter we term as segmental dissymmetry).[29] Due to similar backbone chemistry, HEC and hmHEC have similar segmental dissymmetry and flexibility, but HEC has higher extensibility than hmHEC used in this study. We posit that the higher extensibility of HEC and the presence of stickers on hmHEC chains both influence the contrast observed in rheology and pinching dynamics of the solutions of bare and sticky polymers. Extensional viscosity of finitely extensible nonlinear elastic, with Peterlin's preaveraging approximation (FENE-P) chains in ultradilute solutions can be written as $\eta_E^\infty \rightarrow 3\eta_s + 2\eta_p L_E^2$ exhibiting dependence on both polymer contribution to shear viscosity, η_p, as well as the finite extensibility parameter, $L_E^2 = (R_{max}/R_{us})^2 = N_K^{2(1-\nu)}$, defined as the ratio of the contour length of a chain, $R_{max} = N_K b_K$, to the unstretched length, $R_{us} = \langle R_0 \rangle^{1/2} = N_K^\nu b_K$. Thus, in addition to N_K, the finite extensibility parameter depends on polymer–solvent interactions (including excluded volume interactions)[53] that determine the value of the solvent quality exponent, ν. The value of $L_E^2 \approx 42$ computed for HEC with $M_w = 720$ kg/mol is significantly greater than $L_E^2 \approx 21$ obtained for the semiflexible HEC of $M_w = 300$ kg/mol corresponding to the backbone chain in hmHEC. Thus, a contrast in the pinching dynamics can be anticipated in the TVEC regime due to distinct values of L_E^2 leading to higher η_E^∞ in HEC, even though a more comprehensive model is needed to predict and analyze the overall influence of stickers on effective extensibility as well as extensional rheology response of nondilute associative polymer solutions.

◼ CONCLUSIONS

The shear and extensional rheology response of aqueous dispersions of hydrophobically modified hydroxyethyl cellulose (hmHEC) with $M_w = 300$ kg/mol is contrasted with the response of bare HEC with higher $M_w = 720$ kg/mol. The presence of hydrophobically associating stickers leads to a significant enhancement in zero shear viscosity for hmHEC solutions. Therefore, the specific viscosity of sticky hmHEC solutions at matched concentrations is comparable to values obtained for solutions of higher molecular weight but bare HEC. The specific viscosity of hmHEC solutions exhibits three regimes: $\eta_{sp} \propto c^{1.5}$ for $c < 0.25$ wt. %, $\eta_{sp} \propto c^{3.7}$ in the semidilute, unentangled regime, and $\eta_{sp} \propto c^{4.6}$ in the entangled regime. In contrast, HEC solutions display $\eta_{sp} \propto c^2$ and $\eta_{sp} \propto c^{4.6}$ in semidilute unentangled and entangled regimes, respectively. Semidilute solutions of both polymers exhibit shear thinning at high rates, though a mild shear thickening can be observed in unentangled, semidilute hmHEC solutions at intermediate shear rates. We find that the Cross model can be used to fit the rate-dependent viscosity of hmHEC and the HEC solutions over a wide range of concentrations and shear rates. A combination of associations and clustering leads to a substantial increase in relaxation time of hmHEC solutions, effectively providing the sticky polymer with lower molecular weight ($M_w = 300$ kg/mol) with a similar onset of shear thinning as the bare polymer (HEC, $M_w = 720$ kg/mol) at matched concentration. For the associative polymer, the onset of shear thinning and the relaxation spectrum of associative polymer solutions are influenced both by the sticker association–disassociation time, λ_{sad}, as well as polymer chain and aggregate (micelle/cluster) dynamics. Here, hmHEC solutions exhibit a stronger concentration-dependent increase with $\lambda_s \propto c^{3.4}$ for semidilute solutions.

For both HEC and hmHEC solutions, we show that universal flow curves can be obtained by plotting steady shear viscosity scaled with zero shear viscosity against the product of shear rate and relaxation time (based on Cross model parameters). These curves provide a practical or engineering approximation for rate-dependent viscosity variation that can aid in decision-making in process operations and formulation design. We find that even for cases with nearly matched zero shear viscosity, hmHEC solutions display a higher degree of shear thinning. The observations reiterate the known advantages of utilizing associative polymers as thickeners for formulations ranging from paints and coatings to cosmetics, pharmaceuticals, and food: the formation of hydrophobic associations leads to an enhanced zero shear viscosity that increases the shelf-life and dispersion stability, whereas the disruption of these transient associations provides stronger shear thinning and lower dispersion viscosity under processing conditions. At intermediate deformation rates, shear-induced stretching of subchain segments increases the collision frequency and duration of interchain stickers, increasing the number of elastically active junction points, resulting in mild shear thickening. Plots of steady shear viscosity as a function of shear stress reveal the existence of critical shear stress, τ_c, beyond which fluidity increases, suggesting that at higher concentrations, such associative polymer solution can effectively display yielding and viscoplastic response. The

critical shear stress, τ_c, values show that $\tau_c \propto c^k$ with $k = 1.74$, in agreement with values reported earlier for hydrophobically associating polymers. The higher values of zero shear viscosity and critical stress, τ_c, can reduce the spreading of deposited liquids and gravitational drainage of liquid films, referred to as sagging for paints and coatings. Consequently, in formulation design based on the characterization of shear rheology response, the two polymers would exhibit comparable performance in stabilization and thickening but show contrast in sagging/leveling behavior due to differences in shear-thinning response.

The influence of hydrophobically associating stickers on the pinching dynamics and extensional rheology response was characterized using DoS rheometry. The aqueous hmHEC solutions display a short-terminal, viscoelastocapillary (TVEC) response for all concentrations shown, and a power law regime for entangled solutions arises before the TVEC regime. Unentangled hmHEC solutions display a nearly rate-independent extensional viscosity response for nominally dilute solutions and exhibit mild extensional thickening for semidilute, unentangled solutions that also show mild shear thickening at intermediate shear rates. Entangled hmHEC solutions display a stronger extensional thinning behavior. In all cases, associative polymer dispersions present a greater extensional resistance to pinch-off than the corresponding Newtonian fluid with matched shear viscosity. This delays the final pinch-off event substantially, reducing the size of satellite drops (if present at all) below experimental resolution.

We find that t_{PL} estimated from the power law fits to radius evolution data correlates rather well with the filament lifespan, t_f for the aqueous solutions of both bare and sticky polymers, even though the values of n and n_e (the shear and extensional power law exponents) are quite distinct and appear to be uncorrelated to t_f. Furthermore, t_f for entangled solutions of bare chains is captured rather well by the terminal viscoelastocapillary time, t_{TVEC}. Even though the concentration-dependent values of shear viscosity appear nearly matched for sticky hmHEC and bare HEC polymer solutions, the destruction of transient network structure at high deformation rates leads to significantly smaller terminal extensional viscosity, η_E^∞, and t_{TVEC} values for associative polymer solutions. Tailoring the number of stickers, the strength of the association in transient junctions and controlling the distance between hydrophobic stickers along the hydrophilic backbone each provide possible mechanisms for the design of a stable and sprayable multicomponent complex fluid. In each case, it is essential to characterize and understand the rate-dependent response of the rheologically complex fluid to the large imposed shear and extensional deformation rate characteristic of coating operations. Furthermore, as interactions of hydrophobic stickers with surfactants and other additives can alter the magnitude of their influence, careful investigations of model formulations are needed.[20,38,39,43,105,148,173,174] We anticipate that the results and insights presented in this study will inspire future research into the macromolecular engineering of thickeners or rheology modifiers and formulations.

AUTHOR INFORMATION

Corresponding Author

Vivek Sharma — *Department of Chemical Engineering, University of Illinois at Chicago, Chicago, Illinois 60608, United States;* orcid.org/0000-0003-1152-1285; Email: viveks@uic.edu

Authors

Carina D. V. Martínez Narváez — *Department of Chemical Engineering, University of Illinois at Chicago, Chicago, Illinois 60608, United States*

Jelena Dinic — *Department of Chemical Engineering, University of Illinois at Chicago, Chicago, Illinois 60608, United States*

Xinyu Lu — *Coatings Innovation Center, PPG Industries, Inc., Allison Park, Pennsylvania 15101, United States*

Chao Wang — *Coatings Innovation Center, PPG Industries, Inc., Allison Park, Pennsylvania 15101, United States;* orcid.org/0000-0002-5205-9771

Reza Rock — *Coatings Innovation Center, PPG Industries, Inc., Allison Park, Pennsylvania 15101, United States*

Hao Sun — *Coatings Innovation Center, PPG Industries, Inc., Allison Park, Pennsylvania 15101, United States*

Complete contact information is available at:
https://pubs.acs.org/10.1021/acs.macromol.0c02751

Notes

The authors declare no competing financial interest.

REFERENCES

(1) Winnik, M. A.; Yekta, A. Associative polymers in aqueous solution. *Curr. Opin. Colloid Interface Sci.* **1997**, 2, 424−436.

(2) Larson, R. G. *The Structure and Rheology of Complex Fluids*; Oxford University Press: New York, 1999.

(3) Glass, J. E. *Associative Polymers in Aqueous Media*; American Chemical Society: Washington, D.C., 2000.

(4) Williams, P. A. *Handbook of Industrial and Water Soluble Polymers*; Blackwell Publishing Ltd.: Oxford, 2007.

(5) Sharma, V.; Haward, S. J.; Serdy, J.; Keshavarz, B.; Soderlund, A.; Threlfall-Holmes, P.; McKinley, G. H. The rheology of aqueous solutions of Ethyl Hydroxy-Ethyl Cellulose (EHEC) and its hydrophobically modified Analogue (hmEHEC): Extensional flow response in capillary break-up, jetting (ROJER) and in a cross-slot extensional rheometer. *Soft Matter* **2015**, 11, 3251−3270.

(6) Chassenieux, C.; Nicolai, T.; Benyahia, L. Rheology of associative polymer solutions. *Curr. Opin. Colloid Interface Sci.* **2011**, 16, 18−26.

(7) Rubinstein, M.; Dobrynin, A. V. Associations leading to formation of reversible networks and gels. *Curr. Opin. Colloid Interface Sci.* **1999**, 4, 83−87.

(8) Rubinstein, M.; Semenov, A. N. Dynamics of entangled solutions of associating polymers. *Macromolecules* **2001**, 34, 1058−1068.

(9) Rubinstein, M.; Semenov, A. N. Thermoreversible gelation in solutions of associating polymers. 2. Linear dynamics. *Macromolecules* **1998**, *31*, 1386−1397.

(10) Semenov, A. N.; Rubinstein, M. Thermoreversible gelation in solutions of associative polymers. 1. Statics. *Macromolecules* **1998**, *31*, 1373−1385.

(11) Dooling, L. J.; Tirrell, D. A. Engineering the dynamic properties of protein networks through sequence variation. *ACS Cent. Sci.* **2016**, *2*, 812−819.

(12) Meng, F.; Pritchard, R. H.; Terentjev, E. M. Stress relaxation, dynamics, and plasticity of transient polymer networks. *Macromolecules* **2016**, *49*, 2843−2852.

(13) Hendricks, J.; Louhichi, A.; Metri, V.; Fournier, R.; Reddy, N.; Bouteiller, L.; Cloitre, M.; Clasen, C.; Vlassopoulos, D.; Briels, W. Nonmonotonic Stress Relaxation after Cessation of Steady Shear Flow in Supramolecular Assemblies. *Phys. Rev. Lett.* **2019**, *123*, No. 218003.

(14) Tsitsilianis, C. Responsive reversible hydrogels from associative "smart" macromolecules. *Soft Matter* **2010**, *6*, 2372−2388.

(15) Zhang, Z.; Chen, Q.; Colby, R. H. Dynamics of associative polymers. *Soft Matter* **2018**, *14*, 2961−2977.

(16) Yan, T.; Schröter, K.; Herbst, F.; Binder, W. H.; Thurn-Albrecht, T. What controls the structure and the linear and nonlinear rheological properties of dense, dynamic supramolecular polymer networks? *Macromolecules* **2017**, *50*, 2973−2985.

(17) Martinetti, L.; Carey-De La Torre, O.; Schweizer, K. S.; Ewoldt, R. H. Inferring the nonlinear mechanisms of a reversible network. *Macromolecules* **2018**, *51*, 8772−8789.

(18) Wang, R.; Sing, M. K.; Avery, R. K.; Souza, B. S.; Kim, M.; Olsen, B. D. Classical challenges in the physical chemistry of polymer networks and the design of new materials. *Acc. Chem. Res.* **2016**, *49*, 2786−2795.

(19) Evageliou, V. Shear and extensional rheology of selected polysaccharides. *Int. J. Food Sci. Technol.* **2020**, *55*, 1853−1861.

(20) Clasen, C.; Kulicke, W. M. Determination of viscoelastic and rheo-optical material functions of water-soluble cellulose derivatives. *Prog. Polym. Sci.* **2001**, *26*, 1839−1919.

(21) Tang, S.; Wang, M.; Olsen, B. D. Anomalous self-diffusion and sticky Rouse dynamics in associative protein hydrogels. *J. Am. Chem. Soc.* **2015**, *137*, 3946−3957.

(22) Srivastava, S.; Levi, A. E.; Goldfeld, D. J.; Tirrell, M. V. Structure, Morphology, and Rheology of Polyelectrolyte Complex Hydrogels Formed by Self-Assembly of Oppositely Charged Triblock Polyelectrolytes. *Macromolecules* **2020**, *53*, 5763−5774.

(23) Dinic, J.; Zhang, Y.; Jimenez, L. N.; Sharma, V. Extensional relaxation times of dilute, aqueous polymer solutions. *ACS Macro Lett.* **2015**, *4*, 804−808.

(24) Dinic, J.; Biagioli, M.; Sharma, V. Pinch-off dynamics and extensional relaxation times of intrinsically semi-dilute polymer solutions characterized by dripping-onto-substrate rheometry. *J. Polym. Sci., Part B: Polym. Phys.* **2017**, *55*, 1692−1704.

(25) Dinic, J.; Jimenez, L. N.; Sharma, V. Pinch-off dynamics and dripping-onto-substrate (DoS) rheometry of complex fluids. *Lab Chip* **2017**, *17*, 460−473.

(26) Dinic, J.; Sharma, V. Macromolecular relaxation, strain, and extensibility determine elastocapillary thinning and extensional viscosity of polymer solutions. *Proc. Natl. Acad. Sci. U.S.A.* **2019**, *116*, 8766−8774.

(27) Jimenez, L. N.; Dinic, J.; Parsi, N.; Sharma, V. Extensional relaxation time, pinch-off dynamics and printability of semi-dilute polyelectrolyte solutions. *Macromolecules* **2018**, *51*, 5191−5208.

(28) Jimenez, L. N.; Martínez Narváez, C. D. V.; Sharma, V. Capillary breakup and extensional rheology response of food thickener cellulose gum (NaCMC) in salt-free and excess salt solutions. *Phys. Fluids* **2020**, *32*, No. 012113.

(29) Dinic, J.; Sharma, V. Flexibility, extensibility, and ratio of Kuhn length to packing length govern the pinching gynamics, coil-stretch transition, and rheology of polymer solutions. *Macromolecules* **2020**, *53*, 4821−4835.

(30) Dinic, J.; Sharma, V. Power laws dominate shear and extensional rheology response and capillarity-driven pinching dynamics of entangled hydrodyethyl cellulose (HEC) solutions. *Macromolecules* **2020**, *53*, 3424−3437.

(31) Charpentier-Valenza, D.; Merle, L.; Mocanu, G.; Picton, L.; Muller, G. Rheological properties of hydrophobically modified carboxymethylcelluloses. *Carbohydr. Polym.* **2005**, *60*, 87−94.

(32) Zhao, G. Q.; Chen, S. B. Nonlinear rheology of aqueous solutions of hydrophobically modified hydroxyethyl cellulose with nonionic surfactant. *J. Colloid Interface Sci.* **2007**, *316*, 858−866.

(33) Maestro, A.; Gonzalez, C.; Gutierrez, J. M. Rheological behavior of hydrophobically modified hydroxyethyl cellulose solutions: A linear viscoelastic model. *J. Rheol.* **2002**, *46*, 127−143.

(34) Maestro, A.; Gonzalez, C.; Gutierrez, J. M. Shear thinning and thixotropy of HMHEC and HEC water solutions. *J. Rheol.* **2002**, *46*, 1445−1457.

(35) Landoll, L. M. Non-ionic polymer surfactants. *J. Polym. Sci., Part A: Polym. Chem.* **1982**, *20*, 443−455.

(36) Tanaka, R.; Meadows, J.; Phillips, G. O.; Williams, P. A. Viscometric and spectroscopic studies on the solution behavior of hydrophobically modified cellulose polymers. *Carbohydr. Polym.* **1990**, *12*, 443−459.

(37) González, J. M.; Muller, A. J.; Torres, M. F.; Saez, A. E. The role of shear and elongation in the flow of solutions of semi-flexible polymers through porous media. *Rheol. Acta* **2005**, *44*, 396−405.

(38) Patruyo, L. G.; Muller, A. J.; Saez, A. E. Shear and extensional rheology of solutions of modified hydroxyethyl celluloses and sodium dodecyl sulfate. *Polymer* **2002**, *43*, 6481−6493.

(39) Tirtaatmadja, V.; Cooper-White, J. J.; Gason, S. J. Shear-induced structure and dynamics of hydrophobically modified hydroxy ethyl cellulose (hmHEC) in the presence of SDS. *Korea−Aust. Rheol. J.* **2002**, *14*, 189−201.

(40) Laschet, M.; Plog, J. P.; Clasen, C.; Kulicke, W.-M. Examination of the flow behaviour of HEC and hmHEC solutions using structure−property relationships and rheo-optical methods. *Colloid. Polym. Sci.* **2004**, *282*, 373−380.

(41) Karlberg, M.; Thuresson, K.; Lindman, B. Hydrophobically modified ethyl(hydroxyethyl)cellulose as stabilizer and emulsifying agent in macroemulsions. *Colloids Surf., A* **2005**, *262*, 158−167.

(42) Karlson, L.; Joabsson, F.; Thuresson, K. Phase behavior and rheology in water and in model paint formulations thickened with HM-EHEC: influence of the chemical structure and the distribution of hydrophobic tails. *Carbohydr. Polym.* **2000**, *41*, 25−35.

(43) Nilsson, S.; Thuresson, K.; Lindman, B.; Nystrom, B. Associations in mixtures of hydrophobically modified polymer and surfactant in dilute and semidilute aqueous solutions. A rheology and PFG NMR self-diffusion investigation. *Macromolecules* **2000**, *33*, 9641−9649.

(44) Ganesan, M.; Knier, S.; Younger, J. G.; Solomon, M. J. Associative and entanglement contributions to the solution rheology of a bacterial polysaccharide. *Macromolecules* **2016**, *49*, 8313−8321.

(45) Bataille, I.; Huguet, J.; Muller, G.; Mocanu, G.; Carpov, A. Associative behaviour of hydrophobically modified carboxymethyl-pullulan derivatives. *Int. J. Biol. Macromol.* **1997**, *20*, 179−191.

(46) Afifi, H.; da Silva, M. A.; Nouvel, C.; Six, J.-L.; Ligoure, C.; Dreiss, C. A. Associative networks of cholesterol-modified dextran with short and long micelles. *Soft Matter* **2011**, *7*, 4888−4899.

(47) Payne, G. F.; Raghavan, S. R. Chitosan: a soft interconnect for hierarchical assembly of nano-scale components. *Soft Matter* **2007**, *3*, 521−527.

(48) Kjøniksen, A.-L.; Nyström, B.; Iversen, C.; Nakken, T.; Palmgren, O.; Tande, T. Viscosity of dilute aqueous solutions of hydrophobically modified chitosan and its unmodified analogue at different conditions of salt and surfactant concentrations. *Langmuir* **1997**, *13*, 4948−4952.

(49) Gasbarro, N. M.; Solomon, M. J. Yield stress and rheology of a self-associating chitosan solution. *Rheol. Acta* **2019**, *58*, 729−739.

(50) Nyström, B.; Kjøniksen, A.-L.; Iversen, C. Characterization of association phenomena in aqueous systems of chitosan of different hydrophobicity. *Adv. Colloid Interface Sci.* **1999**, *79*, 81−103.

(51) Wei, Y. P.; Cheng, F. Synthesis and aggregates of cellulose-based hydrophobically associating polymer. *Carbohydr. Polym.* **2007**, *68*, 734−739.

(52) Aubry, T.; Moan, M. Rheological behavior of a hydrophobically associating water soluble polymer. *J. Rheol.* **1994**, *38*, 1681−1692.

(53) McKinley, G. H. Visco-elasto-capillary thinning and break-up of complex fluids. *Rheol. Rev.* **2005**, 1−48.

(54) McKinley, G. H.; Sridhar, T. Filament-stretching rheometry of complex fluids. *Annu. Rev. Fluid Mech.* **2002**, *34*, 375−415.

(55) Petrie, C. J. S. One hundred years of extensional flow. *J. Non-Newtonian Fluid Mech.* **2006**, *137*, 1−14.

(56) Graham, M. D. Interfacial hoop stress and instability of viscoelastic free surface flows. *Phys. Fluids* **2003**, *15*, No. 1702.

(57) Yarin, A. L. *Free Liquid Jets and Films: Hydrodynamics and Rheology*; Longman Scientific & Technical, 1993.

(58) Eggers, J. Nonlinear dynamics and breakup of free-surface flows. *Rev. Mod. Phys.* **1997**, *69*, 865−929.

(59) Eggers, J.; Fontelos, M. A. *Singularities: Formation, Structure, and Propagation*; Cambridge University Press: Cambridge, U.K., 2015; *53*.

(60) Basaran, O. A. Small-scale free surface flows with breakup: Drop formation and emerging applications. *AIChE J.* **2002**, *48*, 1842−1848.

(61) Anna, S. L.; McKinley, G. H. Elasto-capillary thinning and breakup of model elastic liquids. *J. Rheol.* **2001**, *45*, 115−138.

(62) Entov, V. M.; Hinch, E. J. Effect of a spectrum of relaxation times on the capillary thinning of a filament of elastic liquid. *J. Non-Newtonian Fluid Mech.* **1997**, *72*, 31−54.

(63) Stelter, M.; Brenn, G.; Yarin, A. L.; Singh, R. P.; Durst, F. Validation and application of a novel elongational device for polymer solutions. *J. Rheol.* **2000**, *44*, 595−616.

(64) Stelter, M.; Brenn, G.; Yarin, A. L.; Singh, R. P.; Durst, F. Investigation of the elongational behavior of polymer solutions by means of an elongational rheometer. *J. Rheol.* **2002**, *46*, 507−527.

(65) Larson, R. G. The rheology of dilute solutions of flexible polymers: Progress and problems. *J. Rheol.* **2005**, *49*, 1−70.

(66) Nguyen, T. Q.; Kausch, H. H. *Flexible Polymer Chains in Elongational Flow: Theory and Experiment*; Springer-Verlag: Berlin, 1999.

(67) Sridhar, T. An overview of the project M1. *J. Non-Newtonian Fluid Mech.* **1990**, *35*, 85−92.

(68) James, D. F.; Walters, K. A Critical Appraisal of Available Methods for the Measurement of Extensional Properties of Mobile Systems. In *Techniques of Rheological Measurement*; Collyer, A. A., Ed.; Elsevier: New York, 1994; pp 33−53.

(69) Rodd, L. E.; Scott, T. P.; Cooper-White, J. J.; McKinley, G. H. Capillary break-up rheometry of low-viscosity elastic fluids. *Appl. Rheol.* **2005**, *15*, 12−27.

(70) Tan, H.; Tam, K. C.; Tirtaatmadja, V.; Jenkins, R. D.; Bassett, D. R. Extensional properties of model hydrophobically modified alkali-soluble associative (HASE) polymer solutions. *J. Non-Newtonian Fluid Mech.* **2000**, *92*, 167−185.

(71) Odell, J. A.; Keller, A.; Rabin, Y. Flow-induced scission of isolated macromolecules. *J. Chem. Phys.* **1988**, *88*, 4022−4028.

(72) Garrepally, S.; Jouenne, S.; Olmsted, P. D.; Lequeux, F. Scission of flexible polymers in contraction flow: Predicting the effects of multiple passages. *J. Rheol.* **2020**, *64*, 601−614.

(73) Islam, M. T.; Vanapalli, S. A.; Solomon, M. J. Inertial effects on polymer chain scission in planar elongational cross-slot flow. *Macromolecules* **2004**, *37*, 1023−1030.

(74) Vanapalli, S. A.; Ceccio, S. L.; Solomon, M. J. Universal scaling for polymer chain scission in turbulence. *Proc. Natl. Acad. Sci. U.S.A.* **2006**, *103*, 16660−16665.

(75) Meland, H.-G.; Røv-Johnsen, A.; Smistad, G.; Hiorth, M. Studies on surface coating of phospholipid vesicles with a non-ionic polymer. *Colloids Surf., B* **2014**, *114*, 45−52.

(76) Bazilevsky, A. V.; Entov, V. M.; Rozhkov, A. N. In *Liquid Filament Microrheometer and Some of Its Applications*, hird European Rheology Conference and Golden Jubilee Meeting of the British Society of Rheology; Elsevier: Edinburgh, U.K., 1990.

(77) Bazilevsky, A. V.; Entov, V. M.; Rozhkov, A. N. Breakup of a liquid bridge as a method of rheological testing of biological fluids. *Fluid Dyn.* **2011**, *46*, 613−622.

(78) Arnolds, O.; Buggisch, H.; Sachsenheimer, D.; Willenbacher, N. Capillary breakup extensional rheometry (CaBER) on semi-dilute and concentrated polyethyleneoxide (PEO) solutions. *Rheol. Acta* **2010**, *49*, 1207−1217.

(79) Vadillo, D. C.; Mathues, W.; Clasen, C. Microsecond relaxation processes in shear and extensional flows of weakly elastic polymer solutions. *Rheol. Acta* **2012**, *51*, 755−769.

(80) Campo-Deaño, L.; Clasen, C. The slow retraction method (SRM) for the determination of ultra-short relaxation times in capillary breakup extensional rheometry experiments. *J. Non-Newtonian Fluid Mech.* **2010**, *165*, 1688−1699.

(81) Miller, E.; Clasen, C.; Rothstein, J. P. The effect of step-stretch parameters on capillary breakup extensional rheology (CaBER) measurements. *Rheol. Acta* **2009**, *48*, 625−639.

(82) Morozova, S.; Schmidt, P. W.; Metaxas, A.; Bates, F. S.; Lodge, T. P.; Dutcher, C. S. Extensional flow behavior of methylcellulose solutions containing fibrils. *ACS Macro Lett.* **2018**, *7*, 347−352.

(83) Tirtaatmadja, V.; McKinley, G. H.; Cooper-White, J. J. Drop formation and breakup of low viscosity elastic fluids: Effects of molecular weight and concentration. *Phys. Fluids* **2006**, *18*, No. 043101.

(84) Wagner, C.; Amarouchene, Y.; Bonn, D.; Eggers, J. Droplet detachment and satellite bead formation in viscoelastic fluids. *Phys. Rev. Lett.* **2005**, *95*, No. 164504.

(85) Sattler, R.; Gier, S.; Eggers, J.; Wagner, C. The final stages of capillary break-up of polymer solutions. *Phys. Fluids* **2012**, *24*, No. 023101.

(86) Christanti, Y.; Walker, L. M. Surface tension driven jet break up of strain-hardening polymer solutions. *J. Non-Newtonian Fluid Mech.* **2001**, *100*, 9−26.

(87) Christanti, Y.; Walker, L. M. Effect of fluid relaxation time of dilute polymer solutions on jet breakup due to a forced disturbance. *J. Rheol.* **2002**, *46*, 733−748.

(88) Sharma, V.; Ardekani, A. M.; McKinley, G. H. In *'Beads on a String' Structures and Extensional Rheometry Using Jet Break-Up*, 5th Pacific Rim Conference on Rheology (PRCR-5), 2010.

(89) Ardekani, A.; Sharma, V.; McKinley, G. H. Dynamics of bead formation, filament thinning and breakup of weakly viscoelastic jets. *J. Fluid Mech.* **2010**, *665*, 46−56.

(90) Greiciunas, E.; Wong, J.; Gorbatenko, I.; Hall, J.; Wilson, M. C. T.; Kapur, N.; Harlen, O. G.; Vadillo, D.; Threlfall-Holmes, P. Design and operation of a Rayleigh Ohnesorge jetting extensional rheometer (ROJER) to study extensional properties of low viscosity polymer solutions. *J. Rheol.* **2017**, *61*, 467−476.

(91) Mathues, W.; Formenti, S.; McIlroy, C.; Harlen, O. G.; Clasen, C. CaBER vs ROJER-Different time scales for the thinning of a weakly elastic jet. *J. Rheol.* **2018**, *62*, 1135−1153.

(92) Vadodaria, S. S.; English, R. J. Extensional rheometry of cellulose ether solutions: flow instability. *Cellulose* **2016**, *23*, 339−355.

(93) Plog, J. P.; Kulicke, W. M.; Clasen, C. Influence of the molar mass distribution on the elongational behaviour of polymer solutions in capillary breakup. *Appl. Rheol.* **2005**, *15*, 28−37.

(94) Hsiao, K. W.; Dinic, J.; Ren, Y.; Sharma, V.; Schroeder, C. M. Passive non-linear microrheology for determining extensional viscosity. *Phys. Fluids* **2017**, *29*, No. 121603.

(95) Walter, A. V.; Jimenez, L. N.; Dinic, J.; Sharma, V.; Erk, K. A. Effect of salt valency and concentration on shear and extensional rheology of aqueous polyelectrolyte solutions for enhanced oil recovery. *Rheol. Acta* **2019**, *58*, 145−157.

(96) Marshall, K. A.; Liedtke, A. M.; Todt, A. H.; Walker, T. W. Extensional rheometry with a handheld mobile device. *Exp. Fluids* **2017**, *58*, No. 69.

(97) Suteria, N. S.; Gupta, S.; Potineni, R.; Baier, S. K.; Vanapalli, S. A. eCapillary: a disposable microfluidic extensional viscometer for weakly elastic polymeric fluids. *Rheol. Acta* **2019**, *58*, 403−417.

(98) Marshall, K. A.; Walker, T. W. Investigating the dynamics of droplet breakup in a microfluidic cross-slot device for characterizing the extensional properties of weakly-viscoelastic fluids. *Rheol. Acta* **2019**, *58*, 573−590.

(99) Pack, M. Y.; Yang, A.; Perazzo, A.; Qin, B.; Stone, H. A. Role of extensional rheology on droplet bouncing. *Phys. Rev. Fluids* **2019**, *4*, No. 123603.

(100) Murdoch, T. J.; Pashkovski, E.; Patterson, R.; Carpick, R. W.; Lee, D. Sticky but Slick: Reducing Friction Using Associative and Nonassociative Polymer Lubricant Additives. *ACS Appl. Polym. Mater.* **2020**, *2*, 4062−4070.

(101) Rosello, M.; Sur, S.; Barbet, B.; Rothstein, J. P. Dripping-onto-substrate capillary breakup extensional rheometry of low-viscosity printing inks. *J. Non-Newtonian Fluid Mech.* **2019**, *266*, 160−170.

(102) Zhang, Y.; Muller, S. J. Unsteady sedimentation of a sphere in wormlike micellar fluids. *Phys. Rev. Fluids* **2018**, *3*, No. 043301.

(103) Wu, S. J.; Mohammadigoushki, H. Sphere sedimentation in wormlike micelles: Effect of micellar relaxation spectrum and gradients in micellar extensions. *J. Rheol.* **2018**, *62*, 1061−1069.

(104) Omidvar, R.; Wu, S.; Mohammadigoushki, H. Detecting wormlike micellar microstructure using extensional rheology. *J. Rheol.* **2019**, *63*, 33−44.

(105) Jimenez, L. N.; Narváez, C. D. V. M.; Xu, C.; Bacchi, S.; Sharma, V. Rheological Properties Influence Tackiness, Application and Performance of Nail Polish/Lacquer Formulations. *Surface Science and Adhesion in Cosmetics*; John Wiley & Sons, Inc., 2021; pp 109−150.

(106) Chen, Y.-J.; Steen, P. H. Dynamics of inviscid capillary breakup: collapse and pinchoff of a film bridge. *J. Fluid Mech.* **1997**, *341*, 245−267.

(107) Day, R. F.; Hinch, E. J.; Lister, J. R. Self-similar capillary pinchoff of an inviscid fluid. *Phys. Rev. Lett.* **1998**, *80*, 704−707.

(108) Castrejón-Pita, J. R.; Castrejón-Pita, A. A.; Thete, S. S.; Sambath, K.; Hutchings, I. M.; Hinch, J.; Lister, J. R.; Basaran, O. A. Plethora of transitions during breakup of liquid filaments. *Proc. Natl. Acad. Sci. U.S.A.* **2015**, *112*, 4582−4587.

(109) Dinic, J.; Sharma, V. Computational analysis of self-similar capillary-driven thinning and pinch-off dynamics during dripping using the volume-of-fluid method. *Phys. Fluids* **2019**, *31*, No. 021211.

(110) Papageorgiou, D. T. On the breakup of viscous liquid threads. *Phys. Fluids* **1995**, *7*, 1529−1544.

(111) McKinley, G. H.; Tripathi, A. How to extract the Newtonian viscosity from capillary breakup measurements in a filament rheometer. *J. Rheol.* **2000**, *44*, 653−670.

(112) Suryo, R.; Basaran, O. A. Local dynamics during pinch-off of liquid threads of power law fluids: Scaling analysis and self-similarity. *J. Non-Newtonian Fluid Mech.* **2006**, *138*, 134−160.

(113) Doshi, P.; Basaran, O. A. Self-similar pinch-off of power law fluids. *Phys. Fluids* **2004**, *16*, 585−593.

(114) Renardy, M. Similarity solutions for jet breakup for various models of viscoelastic fluids. *J. Non-Newtonian Fluid Mech.* **2002**, *104*, 65−74.

(115) Renardy, M. Self-similar jet breakup for a generalized PTT model. *J. Non-Newtonian Fluid Mech.* **2002**, *103*, 261−269.

(116) Renardy, M. Self-similar breakup of non-Newtonian liquid jets. *Rheol. Rev.* **2004**, *2*, 171−196.

(117) Entov, V. M.; Yarin, A. L. Influence of elastic stresses on the capillary breakup of jets of dilute polymer solutions. *Fluid Dyn.* **1984**, *19*, 21−29.

(118) Clasen, C.; Eggers, J.; Fontelos, M. A.; Li, J.; McKinley, G. H. The beads-on-string structure of viscoelastic threads. *J. Fluid Mech.* **2006**, *556*, 283−308.

(119) Renardy, M. A numerical study of the asymptotic evolution and breakup of Newtonian and viscoelastic jets. *J. Non-Newtonian Fluid Mech.* **1995**, *59*, 267−282.

(120) Fontelos, M. A.; Li, J. On the evolution and rupture of filaments in Giesekus and FENE models. *J. Non-Newtonian Fluid Mech.* **2004**, *118*, 1−16.

(121) Cross, M. M. Rheology of non-Newtonian fluids - A new flow equation for pseudoplastic systems. *J. Colloid Sci.* **1965**, *20*, 417−437.

(122) Oppong, F. K.; De Bruyn, J. R. Microrheology and dynamics of an associative polymer. *Eur. Phys. J. E* **2010**, *31*, 25−35.

(123) Ahn, K. H.; Osaki, K. A network model for predicting the shear thickening behavior of a poly (vinyl alcohol)—Sodium borate aqueous solution. *J. Non-Newtonian Fluid Mech.* **1994**, *55*, 215−227.

(124) Annable, T.; Buscall, R.; Ettelaie, R.; Whittlestone, D. The rheology of solutions of associating polymers: comparison of experimental behavior with transient network theory. *J. Rheol.* **1993**, *37*, 695−726.

(125) English, R. J.; Gulati, H. S.; Jenkins, R. D.; Khan, S. A. Solution rheology of a hydrophobically modified alkali-soluble associative polymer. *J. Rheol.* **1997**, *41*, 427−444.

(126) Esquenet, C.; Terech, P.; Boué, F.; Buhler, E. Structural and rheological properties of hydrophobically modified polysaccharide associative networks. *Langmuir* **2004**, *20*, 3583−3592.

(127) Tam, K. C.; Jenkins, R. D.; Winnik, M. A.; Bassett, D. R. A structural model of hydrophobically modified urethane-ethoxylate (HEUR) associative polymers in shear flows. *Macromolecules* **1998**, *31*, 4149−4159.

(128) Pellens, L.; Ahn, K. H.; Lee, S. J.; Mewis, J. Evaluation of a transient network model for telechelic associative polymers. *J. Non-Newtonian Fluid Mech.* **2004**, *121*, 87−100.

(129) Pellens, L.; Vermant, J.; Mewis, J. Deviations from the stress-optical rule in telechelic associative polymer solutions. *Macromolecules* **2005**, *38*, 1911−1918.

(130) Tan, H.; Tam, K. C.; Jenkins, R. D. Network structure of a model HASE polymer in semidilute salt solutions. *J. Appl. Polym. Sci.* **2001**, *79*, 1486−1496.

(131) Stephanou, P. S.; Tsimouri, I. C.; Mavrantzas, V. G. Two-species models for the rheology of associative polymer solutions: Derivation from nonequilibrium thermodynamics. *J. Rheol.* **2020**, *64*, 1003−1016.

(132) Amin, D.; Wang, Z. Nonlinear rheology and dynamics of supramolecular polymer networks formed by associative telechelic chains under shear and extensional flows. *J. Rheol.* **2020**, *64*, 581−600.

(133) Singh, A.; Mari, R.; Denn, M. M.; Morris, J. F. A constitutive model for simple shear of dense frictional suspensions. *J. Rheol.* **2018**, *62*, 457−468.

(134) Morris, J. F. Shear thickening of concentrated suspensions: Recent developments and relation to other phenomena. *Annu. Rev. Fluid Mech.* **2020**, *52*, 121−144.

(135) Eley, R. R. Applied rheology in the protective and decorative coatings industry. *Rheol. Rev.* **2005**, 173−240.

(136) Eley, R. R. Applied rheology and architectural coating performance. *J. Coat. Technol. Res.* **2019**, *16*, 263−305.

(137) Balmforth, N. J.; Frigaard, I. A.; Ovarlez, G. Yielding to stress: recent developments in viscoplastic fluid mechanics. *Annu. Rev. Fluid Mech.* **2014**, *46*, 121−146.

(138) Blair, G. W. S. Rheology and painting. *Leonardo* **1969**, 51−53.

(139) Lambourne, R.; Striven, T. A. *Paint and Surface Coatings: Theory and Practice*, 2nd ed.; Woodhead Publishing Ltd.: Cambridge, U.K., 1999.

(140) Tam, K. C.; Farmer, M. L.; Jenkins, R. D.; Bassett, D. R. Rheological properties of hydrophobically modified alkali-soluble polymers - Effects of ethylene-oxide chain length. *J. Polym. Sci., Part B: Polym. Phys.* **1998**, *36*, 2275−2290.

(141) Leibler, L.; Rubinstein, M.; Colby, R. H. Dynamics of reversible networks. *Macromolecules* **1991**, *24*, 4701−4707.

(142) English, R. J.; Raghavan, S. R.; Jenkins, R. D.; Khan, S. A. Associative polymers bearing n-alkyl hydrophobes: Rheological evidence for microgel-like behavior. *J. Rheol.* **1999**, *43*, 1175−1194.

(143) Abdala, A. A.; Olesen, K.; Khan, S. A. Solution rheology of hydrophobically modified associative polymers: Solvent quality and hydrophobic interactions. *J. Rheol.* **2003**, *47*, 497−511.

(144) Del Giudice, F.; Tassieri, M.; Oelschlaeger, C.; Shen, A. Q. When microrheology, bulk rheology, and microfluidics meet: Broadband rheology of hydroxyethyl cellulose water solutions. *Macromolecules* **2017**, *50*, 2951−2963.

(145) Kujawa, P.; Audibert-Hayet, A.; Selb, J.; Candau, F. Effect of ionic strength on the rheological properties of multisticker associative polyelectrolytes. *Macromolecules* **2006**, *39*, 384−392.

(146) Regalado, E. J.; Selb, J.; Candau, F. Viscoelastic behavior of semidilute solutions of multisticker polymer chains. *Macromolecules* **1999**, *32*, 8580−8588.

(147) Abdala, A. A.; Wu, W. J.; Olesen, K. R.; Jenkins, R. D.; Tonelli, A. E.; Khan, S. A. Solution rheology of hydrophobically modified associative polymers: Effects of backbone composition and hydrophobe concentration. *J. Rheol.* **2004**, *48*, 979−994.

(148) English, R. J.; Laurer, J. H.; Spontak, R. J.; Khan, S. A. Hydrophobically modified associative polymer solutions: rheology and microstructure in the presence of nonionic surfactants. *Ind. Eng. Chem. Res.* **2002**, *41*, 6425−6435.

(149) Bell, G. I. Models for the specific adhesion of cells to cells. *Science* **1978**, *200*, 618−627.

(150) Tanaka, F.; Edwards, S. F. Viscoelastic properties of physically crosslinked networks:: Part 1. Non-linear stationary viscoelasticity. *J. Non-Newtonian Fluid Mech.* **1992**, *43*, 247−271.

(151) Evans, E.; Ritchie, K. Dynamic strength of molecular adhesion bonds. *Biophys. J.* **1997**, *72*, 1541−1555.

(152) Bustamante, C.; Alexander, L.; Maciuba, K.; Kaiser, C. M. Single-molecule studies of protein folding with optical tweezers. *Annu. Rev. Biochem.* **2020**, *89*, 443−470.

(153) Tripathi, A.; Tam, K. C.; McKinley, G. H. Rheology and dynamics of associative polymers in shear and extension: Theory and experiments. *Macromolecules* **2006**, *39*, 1981−1999.

(154) Tanaka, F. *Polymer Physics: Applications to Molecular Association and Thermoreversible Gelation*; Cambridge University Press, 2011.

(155) Tanaka, F.; Edwards, S. F. Viscoelastic properties of physically crosslinked networks. Transient network theory. *Macromolecules* **1992**, *25*, 1516−1523.

(156) Baxandall, L. G. Dynamics of reversibly crosslinked chains. *Macromolecules* **1989**, *22*, 1982−1988.

(157) Dontula, P.; Pasquali, M.; Scriven, L.; Macosko, C. W. Can extensional viscosity be measured with opposed-nozzle devices? *Rheol. Acta* **1997**, *36*, 429−448.

(158) Cathey, C. A.; Fuller, G. G. Uniaxial and biaxial extensional viscosity measurements of dilute and semi-dilute solutions of rigid rod polymers. *J. Non-Newtonian Fluid Mech.* **1988**, *30*, 303−316.

(159) Gupta, R. K.; Nguyen, D. A.; Sridhar, T. Extensional viscosity of dilute polystyrene solutions: Effect of concentration and molecular weight. *Phys. Fluids* **2000**, *12*, 1296−1318.

(160) Jones, D. M.; Walters, K.; Williams, P. R. On the extensional viscosity of mobile polymer solutions. *Rheol. Acta* **1987**, *26*, 20−30.

(161) Quinzani, L. M.; Armstrong, R. C.; Brown, R. A. Use of coupled birefringence and LDV studies of flow through a planar contraction to test constitutive equations for concentrated polymer solutions. *J. Rheol.* **1995**, *39*, 1201−1228.

(162) Li, X. F.; Denn, M. M. Monte Carlo simulation of steady extensional flows. *J. Rheol.* **2004**, *48*, 805−821.

(163) Wiest, J. M. A differential constitutive equation for polymer melts. *Rheol. Acta* **1989**, *28*, 4−12.

(164) Yaoita, T.; Isaki, T.; Masubuchi, Y.; Watanabe, H.; Ianniruberto, G.; Marrucci, G. Primitive Chain Network Simulation of Elongational Flows of Entangled Linear Chains: Role of Finite Chain Extensibility. *Macromolecules* **2011**, *44*, 9675−9682.

(165) Yaoita, T.; Isaki, T.; Masubuchi, Y.; Watanabe, H.; Ianniruberto, G.; Marrucci, G. Primitive Chain Network Simulation of Elongational Flows of Entangled Linear Chains: Stretch/ Orientation-induced Reduction of Monomeric Friction. *Macromolecules* **2012**, *45*, 2773−2782.

(166) Nielsen, J. K.; Rasmussen, H. K.; Hassager, O.; McKinley, G. H. Elongational viscosity of monodisperse and bidisperse polystyrene melts. *J. Rheol.* **2006**, *50*, 453−476.

(167) Desai, P. S.; Larson, R. G. Constitutive model that shows extension thickening for entangled solutions and extension thinning for melts. *J. Rheol.* **2014**, *58*, 255−279.

(168) Doshi, P.; Suryo, R.; Yildirim, O. E.; McKinley, G. H.; Basaran, O. A. Scaling in pinch-off of generalized Newtonian fluids. *J. Non-Newtonian Fluid Mech.* **2003**, *113*, 1−27.

(169) Huisman, F. M.; Friedman, S. R.; Taborek, P. Pinch-off dynamics in foams, emulsions and suspensions. *Soft Matter* **2012**, *8*, 6767−6774.

(170) Louvet, N.; Bonn, D.; Kellay, H. Nonuniversality in the Pinch-Off of Yield Stress Fluids: Role of Nonlocal Rheology. *Phys. Rev. Lett.* **2014**, *113*, No. 218302.

(171) Coussot, P. Yield stress fluid flows: A review of experimental data. *J. Non-Newtonian Fluid Mech.* **2014**, *211*, 31−49.

(172) Coussot, P.; Gaulard, F. Gravity flow instability of viscoplastic materials: The ketchup drip. *Phys. Rev. E* **2005**, *72*, No. 031409.

(173) Jimenez, L. N.; Narváez, C. D. M.; Xu, C.; Bacchi, S.; Sharma, V. The rheologically-complex fluid beauty of nail lacquer formulations. *Soft Matter* **2021**, *17*, 5197−5213.

(174) Martínez Narváez, C. D. V.; Mazur, T.; Sharma, V. Dynamics and extensional rheology of polymer-surfactant association complexes. *Soft Matter* **2021**, DOI: 10.1039/D1SM00335F.